Seasonal variability of the Ekman transport and pumping in the upwelling system off central-northern Chile (~30°S) based on a high-resolution atmospheric regional model (WRF)

Luis Bravo[1,2,3], Marcel Ramos[2,3,1,6], Orlando Astudillo[1,4], Boris Dewitte[4,3], Katerina Goubanova[5,4]

[1]Centro de Estudios Avanzado en Zonas Áridas (CEAZA), Coquimbo, Chile.
[2]Departamento de Biología, Facultad de Ciencias del Mar, Universidad Católica del Norte, Coquimbo, Chile.
[3]Millennium Nucleus for Ecology and Sustainable Management of Oceanic Islands (ESMOI), Coquimbo, Chile.
[4]Laboratoire d'Etudes en Géophysique et Océanographie Spatiales (LEGOS), Toulouse, France.
[5]Centre Européen de Recherche et de Formation Avancée en Calcul Scientifique (CERFACS), Toulouse, France.
[6]Centro de Innovación Acuícola Aquapacífico, Coquimbo, Chile

Corresponding author: luis.bravo@ucn.cl (L. Bravo), marcel.ramos@ucn.cl (M. Ramos)

Abstract

Two physical mechanisms can contribute to coastal upwelling in eastern boundary current systems, offshore Ekman transport due to the predominant along-shore wind stress and Ekman pumping due to the cyclonic wind stress curl, mainly caused by the abrupt decrease in wind stress (drop-off) in a cross-shore band of 100 km. This wind drop-off is thought to be an ubiquitous feature in coastal upwelling systems and to regulate the relative contribution of both mechanisms. It has been poorly studied along the central-northern Chile region because of the lack in wind measurements along the shoreline and of the relatively low-resolution of the available atmospheric reanalysis. Here, the seasonal variability in Ekman transport, Ekman pumping and their relative contribution to total upwelling along the central-northern Chile region (~30ºS) is evaluated from a high-resolution atmospheric model simulation. As a first step, the simulation is validated from satellite observations, which indicates a realistic representation of the spatial and temporal variability of the wind along the coast by the model. The model outputs are then used to document the fine scale structures in the wind stress and wind curl in relation with the topographic features along the coast (headlands and embayments). Both wind stress and wind curl had a clear seasonal variability with annual and semiannual components. Alongshore wind stress maximum peak occurred in spring, second increase was in fall and minimum in winter. When a threshold of -3×10^{-5} s^{-1} for the across-shore wind curl was considered to define the region from which the winds decrease toward the coast, the wind drop-off length scale varied between 8 and 45 km. The relative contribution of Ekman transport and Ekman pumping to the vertical transport along the coast, considering the estimated wind drop-off length, indicated meridional alternation between both mechanisms, modulated by orography and the intricate coastline. Roughly, coastal divergence predominated in areas with low orography and headlands. Ekman pumping was higher in regions with high orography and the presence of embayments along the coast. In the study region, the vertical transport induced by coastal divergence and Ekman pumping represented 60% and 40% of the total upwelling transport, respectively. The potential role of Ekman pumping on the spatial structure of sea surface temperature is also discussed.

Keywords: drop-off, wind curl, upwelling, Ekman pumping

1. Introduction

In the eastern boundary current systems wind-induced upwelling has mainly been described using two primary mechanisms (Sverdrup et al., 1942; Gill 1982; Pickett and Paduan, 2003; Capet et al., 2004; Jacox and Edwards, 2012). The first one is coastal divergence which is the result of offshore Ekman transport due to alongshore winds (with an equatorward component) and earth's rotation and the presence of the coast (i.e. coastal upwelling). The second one is Ekman pumping which is the result of a cyclonic wind stress curl caused mainly by the wind drop-off that extends only tens of km in width along the coast, and is a typical feature of the eastern boundary current systems (Bakun and Nelson, 1991; Pickett and Paduan, 2003; Capet et al., 2004; Jacox and Edwards, 2012). Starting in the mid 1970s, a series of studies began assessing the contribution of Ekman pumping on coastal upwelling for the California Current System (Halpern, 1976; Nelson, 1977), which later expanded to the other four upwelling systems (Bakun and Nelson, 1991). In one of these four regions, the coast of north and central Chile, this mechanism has been poorly evaluated, primarily due to the scarcity of *in situ* data, limitations in diffusiometer winds that have a "blind zone" near the coast and the relatively low spatial resolution of the atmospheric reanalysis. This has caused a limited progresses in the understanding of the upwelling dynamics and the coastal circulation of the region, among other factors.

Coastal upwelling has been widely studied in several regions of the world, in particular along the Eastern Boundary Upwelling Systems (EBUS). Currently, there is no generalized conceptual model for the upwelling structure that considers the region near the coast, the coastal boundary and the open ocean (Mellor, 1986; Marchesiello and Estrade, 2010). Traditionally a simple relationship based on wind stress along the coast has been used as an index of the coastal upwelling intensity (Bakun, 1973), this approximation does not consider other more complex physical processes, such as the wind curl (Pickett and Paduan, 2003; Capet et al., 2004; Jacox and Edwards, 2012) and the geostrophic flow toward the coast, which is in balance with the along shore pressure gradient and could potentially limit upwelling (Marchesiello et al., 2010; Marchesiello and Estrade, 2010). In the case of the wind curl, several modeling studies from different upwelling systems suggest that wind stress decreases within a narrow coastal band of 10-80 km called wind "drop-off" (Capet et al., 2004; Bane et al., 2005; Perlin et al., 2007; Renault et al., 2012; Renault et al., 2015) that is highly sensitive to the resolution of the model. Thus, regional ocean modeling studies show that the upwelling response is sensitive to the transition in the structure of the wind near the coast (Capet et al., 2004; Jacox and Edwards, 2012), where the structure and physical forcing of the transitional coastal wind profile is not well understood (Jin et al., 2009). In the literature at least three main hypotheses have been proposed to explain the decrease of onshore wind (drop-off) that generates the wind stress curl within the coastal band. The first is related to the change of surface and boundary layer friction in the land-sea interface (Capet et al., 2004). The second is related to the ocean-atmosphere coupling between the sea surface temperature (SST) and the wind (Chelton et al., 2007), particularly cold water upwelling tend to stabilize the atmospheric boundary layer, decoupling the high atmospheric circulation with the surface circulation. The last one is related to coastal orography (Edwards et al., 2001), coastline shape (Perlin et al., 2011), and the combination of both (Renault el at., 2015) constraining the vorticity budget of the low-level atmospheric circulation. Other possible mechanisms that could potentially contribute to wind drop-off near the coast are the effects of sea breeze and pressure gradients (across or along the coast) at sea level.

The central-northern Chile region is characterized by nutrient rich cold surface waters, attributed to the surface circulation of the Humboldt system and mainly coastal upwelling driven by along shore winds that are associated with the southeast Pacific anticyclone (Shaffer et al., 1999; Halpern, 2002). A strong seasonal variability of the southeast Pacific anticyclone produces favorable upwelling winds to peak during spring and summer and decrease during winter (Strub et al., 1998). Within central-northern Chile the area around 30°S is characterized by the most intense upwelling favorable winds (Shaffer et al., 1999; Rutllant and Montecino, 2002). Additionally, local high frequency forcing in the region is associated with atmospheric coastal jets with periods less than 25 days, that are related to synoptic dynamics of the mid-latitude pressure perturbations in this case high pressures, that migrate toward the east (Muñoz and Garreaud, 2005; Rahn and

Garreaud, 2013) and play a major role in coastal upwelling (Renault et al., 2009, 2012; Aguirre et al., 2012). All these features make the region a natural laboratory to explore the forcing mechanisms and describe the physical processes that modulate coastal upwelling.

In a recent modeling study Renault et al. (2012) analyzed the main physical processes that explain changes in sea surface temperature in an upwelling event during the occurrence of an atmospheric coastal jet along the central-northern Chile region. The results showed a clear drop-off of the coastal wind that was not observed in the QuikSCAT data, due to the "blind zone" in the satellite measurements (~25 km offshore). The oceanic response to the atmospheric coastal jet produced significant cooling of the sea surface that significantly contributed to ocean vertical mixing equivalent to the magnitude of the vertical advection near the coast. Their sensitivity analyses showed that the response of the coastal ocean highly depends on the representation of the wind drop-off. This is because the total upwelling (*i.e.* the sum of coastal upwelling and Ekman pumping) depends on the scale of the wind drop-off. The authors suggest that there is a negative effect on coastal upwelling, due to a reduced Ekman transport near the coast that is not balanced by Ekman pumping. In addition, the drop-off has a strong effect on vertical mixing and consequently the cooling of the coastal ocean. In a previous modeling study Capet et al. (2004) off the coast of California suggested that a poor representation of the wind drop-off could underestimate Ekman pumping and overestimate coastal upwelling (and vice versa), with consequences for the coastal circulation processes. Meanwhile, Garreaud et al. (2011) using observations found a local atmospheric coastal jet just north of one of the most prominent geographic points of the region: Punta Lengua de Vaca (see Fig. 1). This coastal jet shows a distinct daily cycle as the result of the strong baroclinicity due to heating differential in the region. In a later study Aguirre et al. (2012) using climatological QuikSCAT winds to force a regional ocean model, found the importance of the wind stress curl over the regional circulation exerting control over the seasonal cycle of an Equatorward coastal jet. This study also evaluated the contribution of Ekman pumping to the total upwelling, which was not well resolved due to a poor resolution of the satellite winds within the first 30 km near the coast. In particular, due to the narrow continental shelf off central-northern Chile, the cells of upwelling due to coastal divergence are trapped near the coast (Estrade et al., 2008), consequently the use of QuikSCAT winds could be overestimating the effect of upwelling driven by coastal divergence and Ekman pumping.

Although previous studies have documented the importance of the wind stress curl near the coast of central Chile (Renault et al, 2012; Aguirre et al, 2012), the impact of the abrupt transition of the wind near the coast (*i.e*. drop-off) and its seasonal variability on upwelling are still poorly understood. Here, prior to addressing this issue from an oceanic perspective, our objective is to document the wind stress curl (drop-off) and its seasonal variability off central-northern Chile (~30°S) using a high resolution (~4 km) atmospheric model. Our focus in on the Ekman pumping and its contribution to the total upwelling, and the factors that could contribute to its meridional variability (*i.e*. topography, coastline and air-sea interactions).

The paper is organized as follow: a description of the atmospheric simulations and the methods used to estimate different upwelling terms are described in section 2. The following section presents results and discussions and was subdivided into three subsections. The first one describes wind stress curl pattern and the spatial scale of the wind drop-off. The second one presents an analysis of the annual variability in Ekman Pumping and coastal divergence, their relationship with coastal topography and their contribution to upwelling transport. Third one, the study relates Ekman Pumping transport to sea surface temperature near the coast. Finally, section 4 presents a summary.

2 Methods and Model Configuration

2.1 Model Output

The Weather Research and Forecasting (WRF) model version 3.3.1 (Skamarock and Klemp, 2008) was configured with three nested domains (Fig. 1) with increasing horizontal grid spacing over the region of interest by a factor of 3 from on domain to the other. The largest synoptic domain covers most of South America and the eastern Pacific in a Mercator projection with a horizontal resolution of 36 km. The second domain covers the coast of north-central Chile (25°-35° S) with a horizontal resolution of 12 km. The innermost domain is centered over the Coquimbo bay system with a horizontal grid spacing of 4 km (Fig. 1). The use of such near-kilometer resolution improves the representation of complex terrain and is necessary for dynamical downscaling of near-surface wind speed climate over complex terrain (Horvath, 2012). WRF employs a terrain-following hydrostatic-pressure coordinate in the vertical, defined as eta (η) levels, here a total of 42 η levels were used in the vertical with increasing resolution toward the surface, 20 of them in the lowest 1.5 km with ~30 m in the vertical for the surface level, such telescopic resolution is a common choice in precedent studies to properly simulate the MBL depth over the ocean (Muñoz and Garreaud, 2005; Rahn and Garreaud 2013; Toniazzo et al, 2013; Renault et al 2012; Rutllant et al, 2013).

Given the complex interactions between alongshore winds, topography, cloudiness, land heating and coastal upwelling in the study region (Rahn and Garreaud 2013; Wood et al., 2011; Toniazzo et al., 2013) we have tested the WRF model in different combinations of parameterizations (cumulus - planetary boundary layer - soil model), surface data (SST forcing, topography and land surface) and nesting technique. A set of eight sensitivity simulations (for more details see response to referee #1, http://www.ocean-sci-discuss.net/os-2015-94/#discussion) was carried out for the control period, i.e. from 1 October 2007 to 31 December 2007 corresponding to the upwelling season in north central Chile. The results were evaluated against surface observations from meteorological automatic stations and scatterometers (QuikSCAT, ASCAT), particular attention was paid to the shoreward decrease and temporal variability of the surface wind speed near the coast. The configuration with the best estimates of observed surface variability and mean state was then used for the long simulation 2007-2012.

The initial and Lateral Boundary and Conditions (LBC) were derived from the National Centers for Environmental Prediction (NCEP) Final Analysis Data (FNL) (Kalnay et al. 1996; available online at http://dss.ucar.edu/datasets/ds083.2/) at 1°x1° global grids every six hours. The boundary conditions are prescribed over the coarser domain with the depth of 5 grid-cells where simulated variables are relaxed towards the FNL solution. The SST forcing data are based on the daily Operational Sea Surface Temperature and Sea Ice Analysis (OSTIA) at 0.05°x0.05° global grids resolution (Stark et al. 2007). The Sea Surface Temperatures (SST) is prescribed at the lower boundary (parent and inner domains) from the OSTIA daily product (Stark et al., 2007). To include the diurnal cycle we have calculated the 6-h anomalies with respect to the daily mean from the six hours FNL SST and then added to the daily OSTIA SST. In this way we generate the 6-h lower boundary updates with the same update rate used for the LBCs as Renault et al. 2015.

For each year the model was re-initialized with the FNL reanalysis every three months leaving 6 overlap days as a spin-up, the outputs during this period were excluded from the analysis, this scheme was suggested by Lo et al. (2008) in order to mitigate the problems of systematic error growth in long integrations and inconsistences between the flow developing and the lateral boundary conditions. The instantaneous model diagnosis were stored at hourly intervals, the time steps were set to 108, 36 and 12 seconds for the domains of 36, 12 and 4 km respectively.

The simulated winds were validated using QuikSCAT and observations from two weather stations near the coast in Loma de Hueso (LDH) and Punta Lengua de Vaca (PLV) and a third station farther inland named Parral Viejo (Fig. 1 and 2). A spatial comparison was done using the coarse resolution grid (36 km) between satellite and WRF winds for 2007-2009. The comparison showed a good agreement between observations and modeling results with a similar spatial structure and magnitudes of the same order, especially within the study region (27ºS-33ºS). The root mean square (RMS) of the difference for observations and model results was less than 1 m s^{-1} (Fig. 2c). The high-resolution model outputs (4 km) were also compared with available observations. Initially, for each of the weather stations daily wind cycles were compared with simulations (not shown). The results indicate a better fit in diurnal variability when the model is forced with SST (OSTIA), which was finally chosen for the simulations performed in this study. The best fit between observations and model outputs was found when the wind intensifies during the afternoon between 17 and 19 hrs. A good model representation of the afternoon winds is key for a proper representation of coastal upwelling in the region. Finally, for each weather station, linear regressions and dispersion plots were done between the meridional component of simulated (4 km) and observed winds (Fig. 2d-f). A good agreement was observed for all the cases.

2.2 Upwelling estimates

The relative importance of coastal upwelling due to coastal divergence (Smith, 1968) was estimated using wind stress obtained by the WRF model:

$$Et = \frac{1}{\rho_w f} \tau \times \hat{k} \quad (1)$$

where Et is Ekman transport ($m^2\ s^{-1}$), τ is the wind stress at the land-sea margin (~4 km from the coast), ρ_w is water density, f is the Coriolis parameter and k is a unit vertical vector. The vertical velocity from Ekman pumping was estimated using a definition given by Halpern (2002) and Renault et al. (2012).

$$w_{EP} = \frac{Curl(\vec{\tau})}{\rho_w f} + \frac{\beta \tau_x}{\rho_w f^2} \quad (2)$$

where $\tau(x,y)$ is wind stress, β is the Coriolis parameter gradient and τ_x is the cross-shore wind stress. Latitude variations were not significant therefore the last term in equation (2) was neglected. In order to compare the two upwelling processes, Ekman pumping was converted into transport by integrating the vertical velocity within a certain distance from the coast, which in our case was the length scale of the wind drop-off (Ld) obtained from a reference value (defined by Renault et al., 2015) where cross-shore wind curl was < -$3x10^{-5}\ s^{-1}$. The wind drop-off spatial length (Ld) varies meridionally (Fig. 3d-c).

Note that if we assume that the wind is parallel to the coast and that the wind curl is dominated by its cross-shore gradient component (and this gradient is nearly constant in the drop-off zone), then the total upwelling transport is simply τ/(ρf) or expressed as vertical velocity is W = τ/(ρfLd), where τ is the wind stress at Ld. Consequently it is apportioned to Ekman transport and pumping according to the amount of drop-off (for more details see Renault et al., 2012). On the other hand, in our study region there is a marked decline toward the coast of the meridional wind component, therefore the wind drop-off has an impact on the total upwelling velocity. Thus a proper assessment of scales involved in both mechanisms is crucial to the upwelling problem.

3 Results and discussion

3.1 Mean wind stress curl and the wind drop-off spatial scale

From the wind stress simulations (model wind outputs) we obtained the mean of the wind stress curl in the three model domains with spatial resolutions of 36, 12 and 4 km (Fig. 3a-c). The mean wind stress curl patterns show clear differences when resolution is increased. In the simulations of higher resolution small scale or finer structures are well defined, especially close to the coast, that are not present in the simulation of coarse resolution, and that are not resolved or studied in previous studies (Aguirre et al., 2012; Renault el al., 2012). The simulations with higher resolution (12 and 4 km) show a cyclonic wind stress curl (negative) within the coastal band and within the Coquimbo bay system that is associated to a positive Ekman pumping (producing upwelling). While in the oceanic sector a less intense anticyclone wind curl predominates. The negative curl within the coastal band is the result of an onshore decay in wind intensity (drop-off) that is characteristic from EBUS systems (Capet et al., 2004; Renault et al., 2012).

In the central-northern Chile region the drop-off length scale (Ld) is between 8 and 45 km (Fig. 3b-c, segmented yellow line). When the resolution of the model is increased, the wind drop-off takes place closer to the coast and exhibits a larger meridional/latitudinal variability, with in particular a larger drop-off scale in the central region of the domain than in the region south of 30.25°S. The meridional differences at Ld could be associated to coastal orography and the shape of the coastline; this will be discussed later in section 3.3. The finer structures in the wind stress curl close to shore, cannot be determined with confidence from observations of the scatterometers of previous and current satellite missions, such as QuikSCAT and/or other satellite, because of the blind zone in measurements within the first 25 km from the shore. Note that the blind zone increases to 50 km when wind stress curl is estimated, as the result of the estimate of the spatial derivative.

Renault et al. (2012) based on atmospheric simulations (obtained with WRF) determined that the extent of the wind drop-off was ~70 km. This length was different from the one obtained in this study (which varied between 8 and 45 km), possibly because of the lower resolution used in their study. To further explain the zonal wind structure and drop-off, Figure 3d shows zonal profiles of the meridional wind of the more exposed region. The results indicate a clear decay of the wind along the coast in the three simulations (36, 12 and 4 km) that is not observed in the satellite data from QuikSCAT. It should be noted the small difference with the satellite product. As mentioned above, in the study region there is a lack of wind information within the coastal band that covers the blind zone of the satellites and that can be used for validation purpose. One of the first in situ measurements in the region were done during the field campaign CupEX (Garreaud et al., 2011). During this experiment a zonal profile of wind was measured using airborne meteorological techniques. These observations allowed detecting an atmospheric coastal jet with a marked daily cycle that extended north of Punta Lengua de Vaca towards the Coquimbo bay system.

Such a coastal jet is present in our simulations that produce a wind curl in the bay system, which affects the circulation and coastal upwelling in the region. Other recent wind observations were collected under the scope of this study (FONDECYT Postdoctoral project 3130671), and are presented in Figure 3e. These wind observations were made with a marine weather station (AirMar) installed on a fishing boat. Measurements were made for 04/22/2014, 05/18/2014, 09/15/2014 and 10/28/2014. Although these measurements do not cover the period of the simulations, they are presented here to illustrate observed features of the zonal wind profiles in the southern region. Despite the large spatial and temporal variability of the observations, they suggest a tendency to a reduction of the along-shore winds toward the coast comparable to what is simulated by the model (Fig. 3d).

Focusing now on the model results, in our study region the atmospheric coastal jet extends from the coast for several tens of kilometers to the west, showing some nearshore maximums, like in Punta Lengua de Vaca (Garreaud and Muñoz, 2005; Muñoz and Garreaud, 2005, among others). In addition, near Punta Lengua de Vaca the atmospheric local and baroclinic jet (local origin), with a marked diurnal cycle has a maximum around 18:00 (local time) (Garraeud et al, 2011; Rahn et al, 2011). We compared the differences between using of WRF wind averaged only during afternoon hours and wind averaged daily during the spring months (not shown). The simulation showed an intensification of the wind in the afternoon, emphasizing the coastal jet at Punta Lengua de Vaca (~30.5°S, south of Tongoy Bay), strong winds were also observed north of Punta Choros (29°S) and south of 31°S. However, when we used the daily averages, we can distinguish the coastal jet and high winds in Punta de Choros and south of 31°S, but with smaller magnitudes than in the afternoon. This is due to the smoothing produced by the averaging to daily mean data. On the other hand, if we look at the structure of Ekman pumping for the two cases, all showed a similar pattern near the coast, with a positive values (favorable to upwelling), but differed in their magnitude, which was greater in the afternoon. Therefore, we believe that for the purposes of this manuscript, using daily averages of wind from the WRF simulation time was valid.

3.2 Annual variability of the wind stress and Ekman pumping

The seasonal analysis of the wind stress and the Ekman pumping is based on the simulation having the highest resolution (4 km), considering the daily average from instantaneous wind values with an hourly sampling over the period between 01/01/2007 and 12/31/2012. Figure 4 presents the mean seasonal cycle of the wind stress for the study area in the coastal fringe extending 150 km from the coast. The wind stress presents a seasonal and spatial variability, with predominance of upwelling favorable winds (with equator-wards component) during all the year round, with maximum values (~0.15 N/m^2) between September and November, which is characteristic of the central-northern region of Chile (Shaffer et al., 1999, Rutllant and Montecino, 2002, Ranh and Garreaud, 2013). The seasonal variability of the wind stress determines the behavior of the coastal upwelling and primary productivity in the region. This is through two main mechanisms, the coastal divergence (by Ekman transport) and the Ekman pumping, that will be evaluated in the following section. The wind can also induce vertical mixing and in turn surface cooling; this could even be of the same order of magnitude as the vertical advection (Renault et al. 2012). In general, these mechanisms may covary in time, responding to the seasonal cycle of the wind stress; hence in a grouped statistical analysis (like SVD) it is difficult to isolate the spatio-temporal combined variability of two mechanisms without rejecting the effect of the third. On the other hand, the model simulates well the coastal atmospheric jet observed in the zone of Punta Lengua de Vaca (~30ºS), in particular the maximum intensity during spring (Rahn and Garreaud, 2011; Rahn and Garreaud, 2013).

Close to the coast, where the satellite data have no coverage or the estimate in wind stress is uncertain (Fig. 1), a wind decay towards the coast (drop-off) is observed during practically all the calendar months of the year, with still a more pronounced tendency in the period between September and December. The horizontal gradient of the wind stress that is most intense close to the coast produces a wind curl with a clockwise rotation direction (cyclonic for the SH) generating a positive Ekman pumping favorable to the upwelling.

In addition to a non-uniform spatial distribution, the drop-off length (Ld) in the area of interest also exhibits a marked seasonal variability. Based on an atmospheric simulation in the west coast of USA, Renault et al. (2015) also suggested that the drop-off presents seasonal and spatial variability, but with an extension ranging from between 10 to 80 km. These authors propose that the drop-off dynamics of the wind is due mainly to orographic effects and the shape of the coastline, reaching a maximal reduction of the wind (~80%) when these are combined. According to these authors, the drop-off length scale of the wind in front of Chile should be approximately 30 km, less than the scale off the west coast of USA. This would result from the different shape of the Chilean coastline characterized by a straighter coastline and the reduced numbers of capes compared to the US West coast. In addition the Andes would induce a sharper onward decline of the wind (drop-off) than the mountains of the west coast of the USA (Renault et al., 2015). In the section 3.3 the length scale of the drop-off along the central-north coast of Chile will be analyzed in relation with the coastal orography and the shape of the coastline.

Despite that the drop-off extension in front of central-northern Chile (~45 km) is on average weaker than that estimated in the California currents system (Enriquez y Friehe, 1996; Renault et al., 2015), the wind-stress curl from this zonal gradient of the wind generates an Ekman pumping with a marked seasonality (Fig. 5) and positive vertical velocities (upward) that reach 4 m day^{-1}, similar values to that obtained by Pickett and Paduan (2003) in front of the region of the California current system.

The simulation (4 km) has allowed to depict and document the mesoscale atmospheric circulation in the first 50 km of the coast (Fig. 3), where the spatial patterns of the Ekman pumping are much more marked, especially at latitudes where there are sharp topographic changes in the coastline (Fig. 5). Thus, structures of Ekman pumping are highlighted to the north of the main headlands of the region (Punta Lengua de Vaca and Punta Choros), and experience a seasonal cycle. In addition, the Ekman pumping presents negative values (downwelling) off shore associated to an anti-cyclonic wind curl around 28.5°S and between 30°S and 31°S that reaches the greatest extent during August, while decreasing considerably in the summer months and beginning of fall (Fig. 5). The difference for the Ekman pumping between the mean spring and the rest of the seasons (*i.e.* summer, fall and winter) indicate that the spring positive pumping dominates the other, specially north of 29ºS, in the interior of the Coquimbo bay system and south of 31.5ºS (not shown).

With the objective of analyzing in more details the seasonal and spatial variability of the wind stress and its zonal gradient, three specific sectors of the study area were selected (28.5º, 30.5º and 32.5ºS), that are outside of the Coquimbo bay system (Fig. 6). As was mentioned before, the region is characterized by a marked wind stress seasonality more pronounced to the south of the study area (Fig. 6c). In general, the wind component along the coast shown a predominance of southerly winds favorable to the upwelling during all the year round, emphasizing a decrease in the wind stress towards the coast for the spring and summer months at 32.5ºS, and in summer at 28.5ºS and 30.5ºS. When estimating the zonal gradient of the wind stress taking as a reference the wind at the coast, the most intense positive gradients (due to the wind drop-off towards the coast) are obtained in a coastal band with a width smaller than 50 km, indicating that the Ekman pumping is the most effective inside the coastal band, as is evidenced in the Figures 4 and 5. On the other hand, the negative zonal gradient extent (Ekman pumping and downwelling) is greater in the sections located farther the north, at 28.5°S and 30.5°S, than in the section located at 32.5°S (Figs. 6 d, e and f), indicating that in the southern part of the study region, the positive Ekman pumping region extends farther than in the zones where the wind stress is more intense seasonally close to the coast (Fig. 4).

3.3 Contributions of Ekman transport and Ekman pumping to the upwelling rate

The central-northern Chile continental shelf is very narrow and very steep so the scale of coastal divergence is <10 km (considering the theoretical framework of Estrade et al., 2008), while the scale of Ekman pumping considering Ld scale (previously defined, based on Renault et al., 2015) is ~45 km. To compare the seasonal contribution of coastal divergence and Ekman pumping to the total transport of coastal upwelling in the study region, the annual cycle of coastal divergence was obtained first by taking the wind of WRF closest to the coast (< 8 km) and meridionally integrated every 0.25° (Fig. 7e), while the annual cycle of Ekman pumping transport (from wind of WRF) was obtained by integrating the vertical velocity from the shoreline to the distance corresponding to the drop-off (Ld) value, also within 0.25° latitude bands (Fig. 7f).

The results indicate a marked annual cycle with maximum vertical transport in the spring, both induced by coastal divergence and Ekman pumping, with secondary maximum in some areas during autumn accounting for a weaker semiannual component. As expected, there is a large temporal coherency along the coast between both processes (the meridional average correlation between Ekman pumping and transport reaches 0.8), except locally at some latitudes (e.g. at 31.25°S) where there is a weak seasonal cycle in Ekman pumping (Fig. 7f) due to either a weak drop-off or a compensation effect by the zonal wind stress component. The high correlations indicate a seasonal consistency between both mechanisms, which has been previously reported in other upwelling systems (e.g. Pickett and Paduan, 2003; Renault et al., 2015). Although both mechanisms are highly correlated at seasonal timescales, they exhibit significant differences in relative magnitude as a function of latitude, *i.e*. when one is intense the other is weak. For instance, coastal divergence strongly dominates over Ekman pumping between 30.25ºS - 31.25ºS (Fig. 7d), which is the most recognized upwelling center in the region (located south of PLV), as well as the region between 28.5°S - 29.25ºS (north of Punta Choros). In those regions Ekman pumping tends to be weaker, while predominant for the area between 29.25 - 30.25ºS, inside the Coquimbo bay system and the area between 28.0ºS - 28.75ºS, north of LDH. South of 31.25°S, both mechanisms vary meridionally more uniformly. The estimate of the meridional correlation between both mechanisms as a function of calendar month indicates that they are better related in spring and summer (~-0.72) than in winter (~0.45). Possible processes that could explain the inverse (negative) spatial relationship between the two mechanisms and its seasonal modulation are discussed below. Before continuing, we should mention that processes such as upwelling shadow can be important in the Coquimbo bay system, and would affect the temperature distribution inside the bay, especially in the southern part of the bay close to the coast, where higher temperatures are observed (and higher thermal front) compared to the lower temperature area that extends north from Punta Lengua de Vaca (Figure 10). In fact a study in the southern part of the Coquimbo bay system (Moraga et al., 2011) shows cyclonic circulation when there are upwelling favorable winds, the circulation is attributed to the separation of oceanic flow in Punta Lengua de Vaca, which is in agreement with the process of upwelling shadow and mainly affects the area indicated above. However, we think that this is not inconsistent with the effect of the wind curl in the area, which would favor upwelling north of Punta Lengua de Vaca. The oceanic response in the area clearly needs more attention and research in the future studies.

Considering the influence of topography and the geometry of the coastline to describe the spatial variability of the wind stress, (e.g. Winant et al., 1988; Burk and Thompson, 1996; Haack, et al., 2001; Koracin et al., 2004; Renault et al., 2015, among others), we now document the relationship between the relative importance of Ekman transport and pumping, and the coastal topography and shape of the coastline in the region. An along-coast orography index (H_{index}) is estimated from the average of the orographic height between the coastline and 100 km inland (as in Renault et al. 2015). In addition, the coastline meandering index (M_{index}) is estimated by converting the position of the coastline into distances and afterward using a high variability-pass filter (with 10 km half- width) the small fluctuations in the index are smoothed, consequently the index only considers the abrupt change in coastline configuration at relatively large scale (Renault et al., 2015). Figure 7a shows the H_{index} (black line) and M_{index} (red line). In the latter index negative values are associated with headlands, while positive values are associated with bays. The drop-off scale and alongshore wind at the coast and at Ld are also included (Fig. 7b-c). Note that Ld is inversely proportional to coastal wind (R^2 de ~0.81), while the wind evaluated at Ld is spatially more homogenous. This differs from the results obtained by Renault et al. (2015) along the western coast of USA. From the inspection of H_{index}, M_{index} and Ld three scenarios are defined that could explain the observed upwelling pattern (Fig. 7d-f):

1. Prevalence of positive Ekman pumping: in sectors such as the Coquimbo bay system and the region north of 28.5ºS (LDH), where the wind curl intensifies due to the sharp decline of onshore wind, with a large drop-off scale (Ld). In addition, the combination of a high orography (large H_{index}) and the presence of bays and headlands along the coastline favor a decrease in the meridional onshore wind.

2. Prevalence of coastal divergence: in sectors characterized by a low topography (small H_{index}) and a negative M_{index} due to the presence of headlands such as Punta Lengua de Vaca and Punta Choros, with a drop-off scale (Ld) smaller and stronger winds alongshore (Fig. 7b-c).

3. South of 31.25°S the pattern is more complex than previous scenarios. Both mechanisms are present but with a slight dominance of coastal divergence on Ekman pumping. South of this latitude, Ld increases, coastal wind decreases and wind curl increases (Fig. 7b-c). M_{index} shows the presence of small inlets and headlands and the orography index is moderate high without largest changes as in the northern coastal region.

Renault et al. (2015) proposed that the coastal topography induces a decrease in the intensity of the wind towards the coast through the vortex stretching term. Similarly, Archer and Jacobson (2005) from atmospheric numerical simulations showed that the topography in the Santa Cruz-California region, is required for the formation of turbulence and vorticity. On the other hand, the shape of the coastline with capes and headlands increases the orographic effect through the vortex stretching term, tilting-twisting and turbulent flux divergence (Archer and Jacobson, 2005; Renault et al., 2015). The sea-land drag coefficient difference mainly acts as a barrier that turns the wind alongshore.

Another minor factor is the sharp coastal sea surface temperature front associated with upwelling. Renault et al (2015) show that in their sensitivity experiment adding a sharp SST front over a coastal band strip leads to weaker surface wind associated with more stable and shallow marine boundary layer. This response of wind may be due to so-called "downward mixing" mechanism (Wallace et al., 1989; Hayes et al., 1989), which was used by many authors to explain the observed tendency of surface winds to decelerate over colder flank of the SST front and accelerate over warmer flank of the SST front (*cf.* Small et al., 2008 and references therein): warm (cold) SST would destabilize (stabilize) the PBL and cause enhanced (reduced) vertical turbulent mixing, increasing (decreasing) downward fluxes of horizontal momentum form the faster flow above to the slower near-surface flow. Nevertheless, a large SST anomaly (by −3 ºC in the experiment of Renault et al., 2015) is needed to induce a significant weakening of wind and significant additional wind drop-off. Therefore, the SST effect can be considered as secondary compared to the orography effect over the California coast.

The combination of coastal topography and the presence of headlands, points and capes on the United State (US) west coast, which induces a stronger and larger wind drop-off, which in turn is associated with a positive Ekman pumping (Koracin et al., 2004; Renault et al., 2015). This characteristic differs from what is observed along central-northern Chile, where the larger drop-off (Ld) length, associated with a strong wind curl (Fig. 7b-c), takes place in the presence of abrupt orography and within the Coquimbo bay system (30.25ºS - 29.25ºS). There the cross-shore wind component is more intense and favors the wind curl, whereas with lower terrain and the presence of headlands the Ld is very small (*cf.* Fig. 10, Renault et al., 2015). The origin of these differences is not well known; they may be due to several factors or processes. For instance, the topographic terrain along the coast of northern Chile is much higher (for the coastal range and Andes mountains) than the terrain along the west coast of the US. Furthermore, a feature of particular interest north of Punta Lengua de Vaca is the presence of the local atmospheric jet, which has a strong diurnal cycle and a clear seasonal variability, as a result of coastal topography that favors baroclinicity north of PLV (Garreaud et al., 2011; Rahn et al., 2011). This feature would deserve further consideration based on the experiments done with the regional atmospheric model, however this is beyond the scope of the present study. Here the focus is on understanding possible effect of the wind drop-off and its spatial and seasonal variability on the upwelling dynamics.

To determine the contribution of the two proposed mechanisms to the total upwelling in the region, vertical transport due to coastal divergence and Ekman pumping were meridionally integrated (from Fig. 7e and 7f, respectively). The contributions of both mechanisms to upwelling (Fig. 8) have a clear annual cycle with a marked semiannual component. Maximum values occur during October, with 0.23 and 0.14 Sv for Ekman transport and Ekman pumping, respectively, while the sum of both is 0.37 Sv. In addition, coastal divergence and Ekman pumping represent 60% and 40% of the total upwelling, respectively. This indicates that Ekman transport is the stronger upwelling mechanism. However, it should be noted that these values are the sum throughout the region, and these percentages would change if specific sectors were considered especially where Ekman pumping has a larger significance (Fig. 7).

Comparing our estimates with those obtained by Aguirre et al. (2012) from QuikSCAT wind information using a larger region (~27.5°S - 40°S), it is observed that coastal divergence from our study is lower, mainly because they estimated averages using only 2 values every day, which may influence the daily mean and therefore their estimates. Also their analysis did not include the wind drop-off area. The winds used in their study are stronger and so are their estimates for coastal divergence (*cf.* Fig. 7, Aguirre et al., 2012). However, for Ekman pumping our results are only slightly smaller than theirs. This difference is mainly due to differences in the method employed to estimate the vertical upwelling transport. In particular they use a length scale (Ld) of 150 km from the coast for their calculation, while in this study a value of 45 km was considered. However, the largest differences in the estimates of the contributions of both mechanisms to total upwelling are in the seasonal variability and the relative contribution to Ekman pumping. The seasonal variability is composed of an annual cycle with a significant semiannual component, whereas that obtained by Aguirre et al., (2012) is rather dominated by the annual cycle. This is because their estimates are based on the average over a larger region that includes the central-southern Chile region, where the wind has a significant annual variability. Moreover, the present results show a higher relative contribution of Ekman pumping to total upwelling in our region. This is partly due to a different technique for estimating this mechanism, the use of different wind products and the differences in the length of both study areas.

3.4 Annual variability of Ekman Pumping and its relationship with Sea Surface Temperature near the coast

A link between SST and wind is found throughout the world's ocean wherever there are strong SST fronts (see review by Xie, 2004; Chelton et al., 2007; Small et al., 2008). This link raises the questions of to what extent the wind-drop off could be associated to marked upwelling fronts in EBUS. In the context of our study, it consists in evaluating the relationship between Ekman pumping and SST, considering that the difficulty to tackle this issue is related to the fact that there is a large temporal coherence between Ekman pumping and transport, preventing a clear identification of Ekman pumping-induced SST anomalies where both processes are in phase. As an attempt to identify regions where Ekman pumping has an imprint on SST, we use the Multi - Scale Ultra - High Resolution SST data set (MUR, http://mur.jpl.nasa.gov) with a spatial resolution of 1 km, which was shown to better capture SST fronts than other products off Peru (Vazquez et al., 2013). Figure 9 shows the annual cycle of the MUR SST. The satellite data were compared to *in situ* observations that were obtained from 13 thermistors positioned close to surface along the coastline between 28ºS–32ºS (these observations were obtained by Centro de Estudios Avanzados en Zonas Aridas, Coquimbo, Chile) covering the period 09/2009–09/2012. The correlations obtained between observations and satellite data were high (0.74-0.94 most values were 0.8) and the RMS between their differences was low varying between 0.54 and 1.3°C. This provided confidence to use MUR temperatures close to the coast in the spatio-temporal analysis done in the study region. The MUR data showed that south of 28.5°S there is a persistent surface cooling through all the year that increases in length (offshore) from ~10 km in the northern region to ~100 km in the southern region. Within this region there are prominent upwelling centers, Punta Lengua de Vaca (~30.5ºS), Punta Choros (~29ºS) and the region between 30.5°S – 33°S. During most of the year a cold surface tongue projects offshore towards the great system of embayments of Coquimbo (with limits between ~29.25°S and 30.25°S), north of Punta Lengua de Vaca. A less intense but with a similar structure is observed north of Punta Loma de Hueso (~28.8ºS).

An illustration of the effect of Ekman pumping on SST is presented in Figure 10 which shows the October mean spatial distribution for wind stress, Ekman pumping, SST and SST gradient. This month was selected because the maximum values of wind stress and increased surface cooling are recorded during this period. During this month, the wind stress (Fig. 10a) was intense with maximum values of ~0.15 Nm^{-2}, showing a clear zonal gradient (drop-off) over the entire coastal band of the study area. Note that the maximum wind stress is north of the two most prominent headlands of the region (PLV and LDH), right where the wind abruptly changes direction, creating an intense cyclonic wind curl north of both ends. As the result from the distribution pattern of the wind stress, wind curl was negative in much of the area of interest resulting in a positive Ekman pumping with vertical velocities of up to 4 m day^{-1} near the coast (Fig. 10b). Also, there are two areas with a slightly negative pumping (light blue regions), following the pattern of the wind stress where the wind decreases away from the coast (see the wind vectors), producing a positive curl and a negative Ekman pumping. Moreover, as mentioned above (see Fig. 7), much of the southern spatial structure in Ekman pumping appears to be associated to the coastal terrain and abrupt changes of the coastline. A good example of this is the tongue-shaped structure that extends from the upwelled waters north of Punta Lengua de Vaca entering the Coquimbo bay system, where the upwelling induced by the Ekman transport seems not affected (Fig. 7). As the result of a positive Ekman pumping, cold water rises to surface causing a decrease in sea surface temperatures in large part of the coastal region (Fig. 10c). However, this cooling is not necessarily caused by Ekman pumping throughout the region, there are other processes that would contribute to the surface cooling that will be discussed later. Despite this, the cooling inside the Coquimbo bay system seems to be caused largely by Ekman pumping. Moreover, outside the Coquimbo bay system high values (>2° C km^{-1}) of the horizontal SST gradient magnitude are distributed in a band near the coast, but not attached to it (Fig. 10d) as expected for upwelling fronts. Within the Coquimbo bay system, there is a homogeneous temperature zone, delimited by a less intense gradient in the west and a greater gradient in the smaller bays of the system, which coincides with the structure of an Ekman pumping tongue projected to the north of Punta Lengua de Vaca.

In order to further document the coupled spatio-temporal patterns of Ekman pumping and the SST field, a Singular Value Decomposition analysis (SVD, Venegas et al., 1997) was performed. The SVD method allows determining statistical modes (time/space) that maximize the covariance between two data sets. Filtered time series (low pass filter with mean half-power of 280 days) and standardized of Ekman pumping and SST-MUR for the 2007-2012 period were analyzed using this method (Fig. 11). In this case the SVD analysis was successful in capturing a dominant seasonal mode. The first dominant mode accounts for 99% of the covariance, with a 43% and 87% of the variance explained by Ekman pumping and SST respectively. Ekman pumping spatial pattern presents maximum values very close to the coast, primarily north of Punta Lengua de Vaca, inside the Coquimbo bay system (29.3ºS–30.2ºS) and north of Punta Choros (28ºS - 29ºS). Also, the pattern is intense near the coast between 30.2ºS (south of PLV) and 32.5°S. The spatial pattern for SST presented areas with high variability associated with areas of maximum Ekman pumping, highlighting the overall variability in the bay system of Coquimbo and the area north of Loma de Hueso (~ 28.8°S). Moreover, the correlation between the time series of expansion coefficient was -0.96 (with R^2 = 0.92 and significant at 95 %), indicating a strong inverse relationship, consistent with that expected for a positive pumping with upward vertical velocities that causes a surface cooling in the region. This results in a greater contribution to the north of headlands in the region (Punta Lengua de Vaca and Loma de Hueso), even within the Coquimbo bay system, which is consistent with the results observed in Figure 7. However, despite the high correlation obtained between both mechanisms within the seasonal scale we cannot infer a relationship with SST only from Ekman pumping, especially where Ekman transport dominates. Also, other processes such as the direct effect of wind must play a significant role, eg. vertical mixing (Renault et al., 2012), or processes related to mesoscale activity (filaments, meanders, eddies, etc.), which are more intense south of Punta Lengua de Vaca (Hormazabal et al., 2004), and/or in general processes related to ocean-atmosphere interaction (Chelton et al., 2007; Renault et al., 2015).

Finally, our analysis calls for more thorough study on the temperature response to wind forcing, which should involve oceanic modeling at a resolution high enough to resolve finer scale processes. The oceanic model could be forced by the high-resolution atmospheric simulations presented in this study, improving in terms of resolution from previous modeling efforts in the region (Renault et al., 2012). The use of a high-resolution coupled ocean-atmosphere model would improve our understanding of the air-sea interactions along our study region. A plan for the development of such model is under way and will be the focus of our next study

4.- Summary

The spatial and temporal variability (annual cycle) of the transport and Ekman pumping, as well as their relative contribution to the total upwelling in the central-northern Chile was studied using winds obtained from a nested configuration of the WRF model allowing to reach 4-km resolution. The simulations showed a cyclonic wind curl (negative) on the coastal-band nearshore and inside the Coquimbo bay system. This negative wind curl is mainly due to the onshore decay of the wind (wind drop-off), which presented length scales (Ld) between 8 and 45 km with a significant latitudinal variability. The wind drop-off scale is in particular larger within 29.25°S-30.25°S and to the north of 28.5°S. When we compared the drop-off scale with other upwelling regions, for example the coast of California (Enriquez and Friehe., 1996; Renault et al, 2015), we find that it is lower in our study region. For instance Ld ranges from 10 and 80 km within 35°N and 45°N (Renault et al., 2015). Despite such difference, the wind stress curl that resulted from this zonal wind shear, generated Ekman pumping with a marked seasonality and vertical velocities at the surface that reached 4 m/day, values comparable to those observed in the California current system.

When comparing the seasonal contribution of coastal divergence and Ekman pumping to the coastal upwelling transport in northern-central Chile, we find that there is a high seasonal coherence between the two mechanisms (> 0.8) with a maximum during spring. However, despite this high seasonal correlation there is a spatial alternation between them, that is, where one is intense the other is weak. This pattern seems to be the result of a close relationship between the topography of the coast, the shape of the coastline and the spatial scale of the wind drop-off. From this information we defined three scenarios that could explain the pattern of upwelling in the area.

Prevalence of positive Ekman pumping associated to large of Ld, observed in regions such as the Coquimbo bay system and north of 28.5ºS. The combination of high terrain and the presence of bays and headlands along the coastline could explain the large Ld values.

- Prevalence of coastal divergence with smaller values of Ld and more intense winds near the coast. This is observed in sectors characterized by a low topography and the presence of headlands as Punta Lengua de Vaca and Punta Choros.

- Combination of both mechanisms where neither divergence nor coastal Ekman pumping dominated over the other. This take place to the south of 31.5°S.

The 3-dimensional aspect of the coastal circulation in the region of interest (Aguirre et al., 2012) prevents a clear identification of the role of each processes on SST variability, although our SVD analysis reveals areas where the similarity of the patterns of Ekman pumping and SST suggests a privileged forcing mechanism like within the Coquimbo bay system and the area north of Loma de Hueso (~ 28.8 °S). Further studies based on the experimentation with an regional oceanic model should be carried out to better identified upwelling regimes by, for instance, using the model winds documented here at different seasons to mimic changes in the drop-off. Considering the rich marine ecosystem hosted by the region (Thiel et al., 2007) our interest goes to relate aspects of the meso to submeso scale circulation (eddies and filaments) to the processes documented in this study. This is planned for future work.

Finally, the model allowed for an estimate of the near-shore (coastal frange of ~50km) low-level circulation and, evidences fine scale structure of the wind stress curl that cannot be estimated from satellite observations. Considering the overall realism of the model simulation, our study could be used to guide field experiments and gather in situ measurements in order to gain further knowledge in the processes that constrain such features

Acknowledgements

This work was financed by Postdoctoral FONDECYT/Chile Nº 3130671 and support from Centro de Estudios Avanzados en Zonas Aridas (CEAZA), Coquimbo, Chile. M. Ramos, L. Bravo and B. Dewitte acknowledge support from FONDECYT (project 1140845) and Chilean Millennium Initiative (NC120030). B. Dewitte and M. Ramos acknowledge support from FONDECYT (project 1151185). CNES (Centre National d'Etudes Spatiales, France) is thanked for financial supports through the OSTST project EBUS-South. Katerina Goubanova was supported by IRD. The contribution from two reviewers and the editor is deeply appreciated; their comments and suggestions improved and strengthen this study

5.- References

Aguirre, C., Pizarro, O., Strub, P. T., Garreaud, R. and Barth, J.A.: Seasonal dynamics of the near-surface alongshore flow off central Chile, J. Geophys. Res., 117, C01006, doi:10.1029/2011JC007379, 2012.

Archer, C. L. and Jacobson, M. Z.: The Santa Cruz Eddy. Part II: Mechanisms of Formation, Mon. Weather Rev., 133(8), 2387–2405, doi:10.1175/MWR2979.1, 2005.

Bakun, A.: Coastal upwelling indices, west coast of North America, 1946-71. U.S.Dep. Commer., NOAA Tech. Rep., NMFS SSRF-671, 103 p., 1973.

Bakun, A. and Nelson, C.: The seasonal cycle of wind stress curl in subtropical Eastern boundary current regions. J. Phys. Oceanogr., 21: 1815-1834, 1991.

Bane, J. M., Levine, M. D., Samelson, R. M., Haines, S. M., Meaux, M. F., Perlin, N., Kosro, P. M. and Boyd, T.: Atmospheric forcing of the Oregon coastal ocean during the 2001 upwelling Season, J. Geophys. Res., 110.C10S02, 2005.

Beljaars, A.C.M.: The parameterization of surface fluxes in large-scale models under free convection. Quart. J. Roy. Meteor. Soc., 121, 255–270, 1994.

Bretherton, C. S. and Park, S.: A new moist turbulence parameterization in the Community Atmosphere Model. J. Climate, 22, 3422–3448, 2009.

Burk, S. D. and Thompson, W. T. : The summertime low-level jet and marine boundary layer structure along the California coast. Mon. Weather Rev., 124, 668–686, 1996.

Capet, X. J., Marchesiello, P. and McWilliams, J. C.: Upwelling response to coastal wind profiles, Geophys. Res. Lett., 31, L13311, 2004.

Chelton, D. B., Schlax, M. G. and Samelson, R. M.: Summertime coupling between sea surface temperature and wind stress in the California Current System, J. Phys. Oceanogr., 37, 495-517, 2007.

Dyer, A. J. and Hicks, B. B.: Flux–gradient relationships in the constant flux layer. Quart. J. Roy. Meteor. Soc., 96, 715–721, 1970

Edwards K.A., Rogerson A.M., Winant C.D. and Rogers D.P.: Adjustment of the marine atmospheric boundary layer to a coastal cape, J Atmos Sci 58(12):1511–1528, 2001.

Enriquez, A.G. and Friehe, C.A. : Effects of Wind Stress and Wind Stress Curl Variability on Coastal Upwelling J. Phys. Oceanogr., 25, 1651-1671, 1996.

Estrade, P., Marchesiello, P., Colin de Verdiere, A. and Roy, C.: Cross-shelf structure of coastal upwelling: A two-dimensional expansion of Ekman's theory and a mechanism for inner shelf upwelling shut down, J. Mar. Res., 66, 589–616, doi:10.1357/002224008787536790, 2008.

Garreaud, R. and Muñoz, R.: The low-level jet off the subtropical west coast of South America: Structure and variability, Mon. Weather Rev., 133, 2246–2261, doi:10.1175/MWR2972.1, 2005.

Garreaud R, Rutllant, J., Muñoz, R., Rahn, D., Ramos, M. and Figueroa, D.: VOCALS-CUpEx: The Chilean Upwelling Experiment, Atmos. Chem. Phys., 11, 2015–2029, doi:10.5194/acp-11-2015-2011, 2011.

Gill, A.E.: Atmosphere–ocean dynamics, International Geophysics Series 30, 403pp, 1982.

Haack, T., Burk, S. D., Dorman, C. and Rogers, D.: Supercritical Flow Interaction within the Cape Blanco–Cape Mendocino Orographic Complex, Mon. Weather Rev., 129, 688–708, 2001.

Halpern, D.: Measurements of near-surface wind stress over an upwelling region near the Oregon coast, J. Phys. Oceanogr., 6, 108–112, 1976.

Halpern, D.: Offshore Ekman transport and Ekman pumping off Peru during the 1997–1998 El Niño, Geophys. Res. Lett., 29(5), 1075, doi:10.1029/2001GL014097, 2002.

Hayes, S. P., McPhaden, M. J. and Wallace, J. M.: The influence of sea surface temperature on surface wind in the eastern equatorial Pacific: weekly to monthly variability. J. Climate 2, 1500–1506. 1989.

Hong, S. Y. and Lim, J.O.: The WRF single–moment 6–class microphysics scheme (WSM6). J. Korean Meteor. Soc., 42, 129–151, 2006.

Hormazabal, S., Shaffer, G. and Leth, O.: Coastal transition zone off Chile, J. Geophys. Res., 109, C01021, doi:10.1029/2003JC001956, 2004.

Horvath, K., Koracin, D., Vellore, R., Jiang, J. and Belu, R.: Sub-kilometer dynamical downscaling of near-surface winds in complex terrain using WRF and MM5 mesoscale models, J. Geophys. Res., 117, D11111, doi:10.1029/2012JD017432, 2012.

Iacono, M. J., Delamere, J. S., Mlawer, E. J., Shephard, M. W., Clough, S. A. and Collins, W. D.: Radiative forcing by long–lived greenhouse gases: Calculations with the AER radiative transfer models. J. Geophys. Res., 113, D13103, 2008

Jacox, M. G. and Edwards, C. A.: Upwelling source depth in the presence of nearshore wind stress curl, J. Geophys. Res., 117, C05008, doi:10.1029/2011JC007856, 2012.

Janjic, Z. I.: Comments on ‘‘Development and evaluation of a convection scheme for use in climate models.’’ J. Atmos. Sci., 57, 3686–3686, 2000.

Jin, X., Dong, C., Kurian, J., McWilliams, J. C., Chelton, D. B. and Li. Z.: SST-Wind Interaction in Coastal Upwelling: Oceanic Simulation with Empirical Coupling, J. Phys. Oceanogr. 39:11, 2957-2970, 2009.

Kalnay, E., and Coauthors: The NCEP/NCAR 40-Year Re- analysis Project. Bull. Amer. Meteor. Soc., 77, 437–471, 1996.

Koračin, D., Dorman, C. E. and Dever, E. P.: Coastal Perturbations of Marine-Layer Winds, Wind Stress, and Wind Stress Curl along California and Baja California in June 1999, J. Phys. Oceanogr., 34(5), 1152–1173, doi:10.1175/1520-0485(2004)034<1152:CPOMWW>2.0.CO;2, 2004.

Lo, J. C.-F., Yang, Z.-L. and Pielke, R. A. Sr.: Assessment of three dynamical climate downscaling methods using the Weather Research and Forecasting (WRF) model. J. Geophys. Res., 113, D09112, doi:10.1029/2007jd009216, 2008.

Marchesiello, P. and Estrade, P.: Upwelling limitation by geostrophic onshore flow, J. Mar. Res., 68, 37–62, doi:10.1357/002224010793079004, 2010.

Marchesiello P., Lefevre, L., Vega, A., Couvelard, X. and Menkes, C.: Coastal upwelling, circulation and heat balance around New Caledonia’s barrier reef. Mar. Poll. Bull. 61, 432– 448, 2010.

Mellor, G. L.: Numerical simulation and analysis of the mean coastal circulation off California, Cont. Shelf Res., 6, 689 –713, 1986.

Moraga-Opazo, J., Valle-Levinson, A., Ramos, M. and Pizarro-Koch, M.: Upwelling-Triggered near-geostrophic recirculation in an equatorward facing embayment, Cont. Shelf Res., 31: 1991–1999, doi: 10.1016/j.csr.2011.10.002, 2011.

Muñoz, R. and Garreaud, R.: Dynamics of the low-level jet off the subtropical west coast of South America, Mon. Weather Rev., 133, 3661–3677, doi:10.1175/MWR3074.1, 2005.

Nelson, C.S.: Wind stress and wind-stress curl over the California Current, NOAA Tech. Rep., NMFS SSRF-714, U.S. Dept. of Commerce, 87 pp, 1977.

Paulson, C. A.: The mathematical representation of wind speed and temperature profiles in the unstable atmospheric surface layer. J. Appl. Meteor., 9, 857–861, 1970.

Perlin, N., Skyllingstad, E., Samelson, R. and Barbour, P.: Numerical simulation of air-sea coupling during coastal upwelling, J. Phys. Oceanogr., 37(8), 2081–2093, doi:10.1175/JPO3104.1, 2007.

Perlin N., Skyllingstad E.D. and Samelson, R.M.: Coastal atmospheric circulation around an idealized cape during wind-driven upwelling studied from a coupled ocean-atmosphere model. Mon Weather Rev 139(3), 809–829, 2011.

Pickett, M. and Paduan, J.D.: Ekman transport and pumping in the California Current based on the U.S. Navy's high-resolution atmospheric model (COAMPS), J. Geophys. Res., 108, C10 3327, doi: 10.1029/2003JC001902, 2003.

Rahn D.A., Garreaud R. and Rutllant J.: The low-level atmospheric circulation near Tongoy Bay / point Lengua de Vaca (Chilean coast 30°S), Mon. Wea. Rev., 139: 3628–3647, doi: 10.1175/MWR-D-11-00059.1, 2011.

Rahn, D. and Garreaud, R.: A synoptic climatology of the near-surface wind along the west coast of South America, Int. J. Climatol., 34 doi: 10.1002/joc.3724, 2013.

Renault, L., Dewitte, B., Falvey, M., Garreaud, R., Echevin, V. and Bonjean, F.: Impact of atmospheric coastal jet off central Chile on sea surface temperature from satellite observations (2000–2007), J. Geophys. Res., 114, C08006, doi:10.1029/2008JC005083, 2009.

Renault, L., Dewitte, B., Marchesiello, P., Illig, S., Echevin, V., Cambon, G., Ramos, M., Astudillo, O., Minnis, P., and Ayers, J. K.: Upwelling response to atmospheric coastal jets off central Chile: A modeling study of the October 2000 event, J. Geophys. Res., 117, C02030, doi:10.1029/2011JC007446, 2012.

Renault, L., Hall, H. and McWilliams. J.C.: Orographic shaping of US West Coast wind profiles during the upwelling season. Clim. Dyn., doi: 10.1007/s00382-015-2583-4, 2015

Rutllant, J. and Montecino,V.: Multiscale upwelling forcing cycles and biological response off north-central Chile. Revista Chilena de Historia Natural 75: 217-231, 2002.

Rutllant, J. A., Muñoz, R. C. and Garreaud, R. D.: Meteorological observations on the northern Chilean coast during VOCALS-REx. Atmos. Chem. Phys., 13, 3409–3422, doi:10.5194/acp-13-3409-2013, 2013

Shaffer, G., Hormazabal, S., Pizarro, O., Djurfeldt, L. and Salinas, S.: Seasonal and interannual variability of currents and temperature over the slope off central Chile, J. Geophys. Res., 104, 29,951–29,961, doi:10.1029/1999JC900253, 1999.

Skamarock, W. C. and Klemp, J. B.: A time-split nonhydrostatic atmospheric model for weather research and forecasting applications, J. Comput. Phys., 227, 3465–3485, doi:10.1016/j.jcp.2007.01.037, 2008.

Small, R. J., deSzoeke, S.P., Xie, S.P., O'Neill, L., Seo, H., Song, Q., Cornillon, P., Spall, M. and Minobe, S.: Air-sea interaction over ocean fronts and eddies. Dyn. Atmos. Oceans, 45, 274–319, 2008.

Smith, R.L.: Upwelling, Oceanogr. Mar. Bio. Ann. Rev., 6, 11-46, 1968.

Stark, J. D., Donlon, C. J., Martin, M. J. and McCulloch, M. E.: OSTIA: An operational, high resolution, real time, global sea surface temperature analysis system. OCEANS 2007-Europe, IEEE, 1–4, 2007.

Strub, P. T., Montecino, V., Rutllant, J. and Salinas, S.: Coastal ocean circulation off western south America, in The Sea, vol. 11, The Global Coastal Ocean: Regional Studies and Syntheses, edited by A. R. Robinson and K. H. Brink, pp. 273– 314, John Wiley, New York, 1998.

Sverdrup, H. U.: Wind-driven currents in a baroclinic ocean, with application to the equatorial currents of the eastern Pacific. Proc. Natl. Acad. Sci. USA, 33, 318–326, 1947.

Tewari, M., Chen, F., Wang, W., Dudhia, J., LeMone, M. A., Mitchell, K., Gayno, M. Ek, G., Wegiel, J. and Cuenca, R. H.: Implementation and verification of the unified NOAH land surface model in the WRF model. 20th conference on weather analysis and forecasting/16th conference on numerical weather prediction, pp. 11–15, 2004

Thiel, M., Macaya, E. ., Acuña, E., Arntz, W. E., Bastias, H., Brokordt, K., Camus, P. A., Castilla, J. C., Castro, L. R., Cortés, M., Dumont, C. P., Escribano, R., Fenández, M., Gajardo, J. A., Gaymer, C. F., Gómez, I., González, A. E., González, H., Haye, P. A., Illanes, J. C., Iriarte, J. L., Lancellotti, D. A., Luna-Jorquera, G., Luxoro, C., Manriquez, P. H., Marín, V., Muñoz, P., Navarrete, S. A., Perez, E., Poulin, E., Sellanes, J., Sepúlveda, H. H., Stotz, W., Tala, F., Thomas, A., Vargas, C. A., Vasquez, J. A. and Vega, J. M. A.: the Humboldt Current System of Northern-Central Chile Oceanographic Processes , Ecological Interactions, edited by R. N. Gibson, R. J. A. Atkinson, and J. D. M. Gordon, Oceanogr. Mar. Biol. An Annu. Rev., 45(3), 195–344, doi:Book_Doi 10.1201/9781420050943, 2007.

Toniazzo, T., Sun, F., Mechoso, C. R. and Hall, A.: A regional modeling study of the diurnal cycle in the lower troposphere in the south-eastern tropical Pacific. Clim. Dyn., 41,1899–1922, doi:10.1007/s00382-012-1598-3, 2013.

Vazquez-Cuervo, J., Dewitte, B., Chin, T. M., Amstrong, E., Purca, S. and Alburqueque, E.: An analysis of SST gradient off the Peruvian coast; The impact of going to higher resolution, Remote Sensing of Environment, 131, 76-84, 2013.

Venegas, S.A, Mysak, L.A. and Straub, D.N.: Atmosphere-Ocean Coupled Variability in the South Atlantic. Journal of Climate, 10, 2904-2920, 1997.

Webb, E. K.: Profile relationships: The log-linear range, and extension to strong stability. Quart. J. Roy. Meteor. Soc., 96, 67–90, 1970.

Wallace, J., Mitchell, T. and Deser, C.: The influence of sea-surface temperature on surface wind in the eastern equatorial Pacific: Seasonal and interannual variability. J. Climate, 2, 1492–1499, 1989.

Winant, C.D., Dorman, C.E., Friehe, C.A. and Beardsley, R.C.: The marine layer off Northern California: an example of supercritical channel flow. J. Atmos. Sci. 45, 3588–3605, 1988.

Wood, R., Mechoso, C. R., Bretherton, C. S., Weller, R. A., Huebert, B., Straneo, F., Albrecht, B. A., Coe, H., Allen, G., Vaughan, G., Daum, P., Fairall, C., Chand, D., Gallardo Klenner, L., Garreaud, R., Grados, C., Covert, D. S., Bates, T. S., Krejci, R., Russell, L. M., de Szoeke, S., Brewer, A., Yuter, S. E., Springston, S. R., Chaigneau, A., Toniazzo, T., Minnis, P., Palikonda, R., Abel, S. J., Brown, W. O. J., Williams, S., Fochesatto, J., Brioude, J. and Bower, K. N.: The VAMOS Ocean-Cloud-Atmosphere-Land Study Regional Experiment (VOCALS-REx): goals, platforms, and field operations. Atmos. Chem. Phys., 11, 627–654, doi:10.5194/acp-11-627-2011, 2011.

Xie, S.P.: Satellite observations of cool ocean-atmosphere interaction. Bull Amer. Meteor. Soc., 85:195-208, 2004.

Zhang, D. L., and Anthes, R.A.: A high–resolution model of the planetary boundary layer– sensitivity tests and comparisons with SESAME–79 data. J. Appl. Meteor. 21, 1594–1609, 1982. 1982,

Table 1: Information of the physics options and main features used in the simulations.

Parameterization	References
Microphysics: WRF Single-Moment 6-class scheme. A scheme with ice, snow and graupel processes suitable for high-resolution simulations.	(Hong et al. 2006)
Longwave/Shortwave radiation: Rapid Radiative Transfer Model (RRTMG). An accurate scheme using look- up tables for efficiency, accounts for multiple bands, trace gases, and microphysics species. It includes the Monte Carlo Independent Column Approximation MCICA method of random cloud overlap.	(Iacono et al. 2008).
Boundary layer: University of Washington Turbulent kinetic energy (TKE) Boundary Layer scheme. This scheme is TKE based, and it is characterized by the use of moist-conserved variables, an explicit entrainment closure, downgradient diffusion of momentum, and con- served scalars within turbulent layers.	(Bretherton and Park 2009)
Surface layer: Based on Monin-Obukhov with Carslon-Boland viscous sub-layer and standard similarity functions from look-up tables.	(Paulson, C. A., 1970) (Dyer, A. J. et al., 1970) (Webb, E. K., 1970) (Beljaars, A.C.M., 1994) (Zhang and Anthes 1982)
Land surface model: The NOAH Land Surface Model. For land surface processes including vegetation, soil, snowpack and land atmosphere energy, momentum and moisture exchange.	(Tewari, M. et al., 2004)
Cumulus: Betts-Miller-Janjic scheme. Operational Eta scheme. Column moist adjustment scheme relaxing towards a well-mixed profile.	(Janjic, Z. I., 2000)

FIGURE CAPTIONS

Figure 1. Study area showing bathymetry and topography of the coastal terrain. The dotted thick line indicates the western boundary of the coastal band where satellite information (~25 km offshore) is absent. Red squares indicate the location of the three weather stations at Loma de Hueso, Punta Lengua de Vaca and Parral Viejo. The inset plot shows the three model domains used in the WRF simulations (36, 12 and 4 km).

Figure 2. Comparisons of the spatial patterns of the mean velocity fields of winds obtained (to same period 2007-2009) from a) QuikSCAT b) WRF simulation for the 36 km grid configuration. c) Root Mean Square (RMS) differences between observations and model results. The lower panels show dispersion plots between the observed and modeled N-S winds at d) Loma de Hueso, e) Parral Viejo and f) Punta Lengua de Vaca (Fig.1). Red line represent to linear regress and black line is 1:1 relation.

Figure 3. Mean wind stress curl obtained by the model (from 2007-2012) using three model domains a) 36 km, b) 12 km and c) 4 km. The yellow dotted line represents the length scale of the wind drop-off determined from a threshold value of -0.3 x 10^{-4} s^{-1} (Renault et al., 2015). d) Mean zonal profiles of alongshore wind speed obtained from the three model configurations (36, 12 and 4 km) and QuikSCAT observations are shown. e) Zonal profiles of alongshore wind speed from a weather station obtained onboard of a fishing boat during 22 April (black line), 18 May (black dashed line), 15 September (red line) and 28 October (red dashed line) of 2014 are also shown. The segmented line in d) and e) indicates the location of the satellite blind spot.

Figure 4. Wind stress annual cycle obtained from the simulation at 4 km resolution (from 2007-2012). Color represents the magnitude of wind stress (in Nm^{-2}) and the arrows indicate the wind stress direction.

Figure 5. Annual cycle of Ekman pumping (vertical velocity in md^{-1}) obtained from the simulation at 4 km resolution (from 2007-2012).

Figure 6. Hovmoller diagrams of alongshore wind stress seasonal cycle (top panels) and the zonal gradient of alongshore wind (lower panels) for the regions at 28.5ºS (a, d), 30.5ºS (b, e) y 32.5ºS (c, f). The monthly mean zonal wind stress and mean zonal gradient are also shown (side black line).

Figure 7. Contributions of the Ekman transport and Ekman pumping to the vertical transport near the coast. a) Integrated orography index (H_{index}, black line) and coastaline meander index (M_{index}, red line, see text). b) Drop-off spatial length. c) Alongshore wind at Ld (red line) and coastal (black line). d) Ratio between Ekman pumping and Ekman transport e) Seasonal vertical transport associated with Ekman transport and f) seasonal vertical transport associated with Ekman pumping. To estimate the Ekman transport the wind stress closest to the coast was used, while Ekman pumping was integrated from the coast to the longitude corresponding to a distance from the coast equal to the length of the drop-off (see text).

Figure 8. Contributions of Ekman transport and Ekman pumping to the vertical transport near the coast (in Sv) over the study area (27.75°S-32.5°S, see Fig. 7). Seasonal vertical transport associated with Ekman transport (black line), Ekman pumping (red line) and total wind induced vertical transport (blue line, sum of both vertical transports). The estimates were carried out from the WRF simulation at 4 km resolution.

Figure 9. Annual cycle of sea surface temperature obtained using data from the Multi-scale Ultra-high Resolution (MUR). Top and bottom panels used a different colormap scale.

Figure 10. October mean spatial distribution for a) wind stress and b) Ekman pumping using the 4 km grid spacing simulation and c) sea surface temperature (SST) and d) SST gradient obtained from MUR observations.

Figure 11. First SVD mode between Ekman pumping (WEk) from the WRF simulation at 4 km resolution and sea surface temperature (SST) from MUR data. a) The Ekman

pumping spatial component. b) The SST spatial component. c) The black (red) line represents the associated Ekman pumping (SST) time series. Note that the units are arbitrary.

FIGURES

Figure 1.

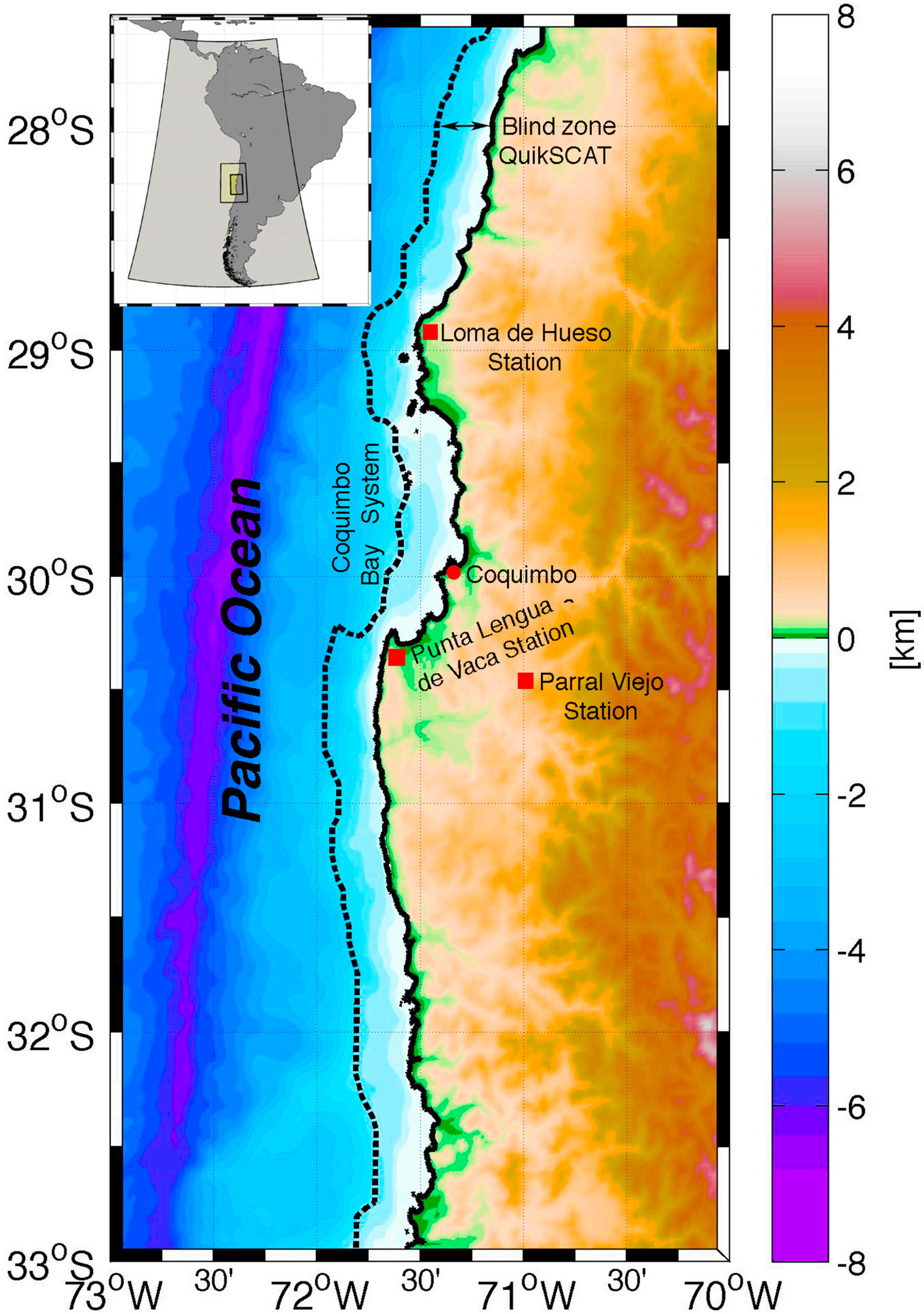

Figure 2.

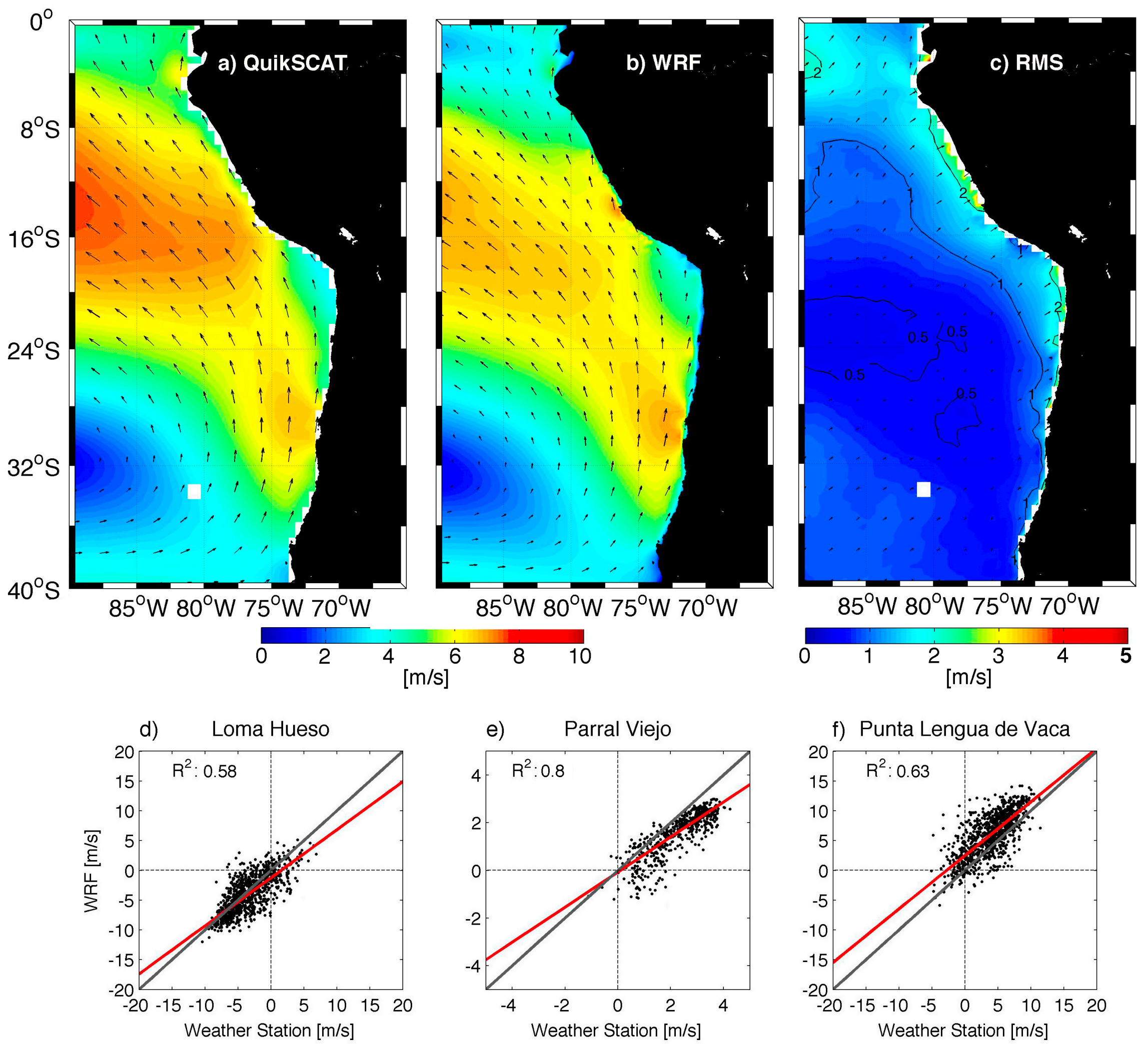

a) QuikSCAT
b) WRF
c) RMS
0°
8°S
16°S
24°S
32°S
40°S
85°W 80°W 75°W 70°W
[m/s]
d) Loma Hueso
e) Parral Viejo
f) Punta Lengua de Vaca
R²: 0.58
R²: 0.8
R²: 0.63
WRF [m/s]
Weather Station [m/s]

Figure 3.

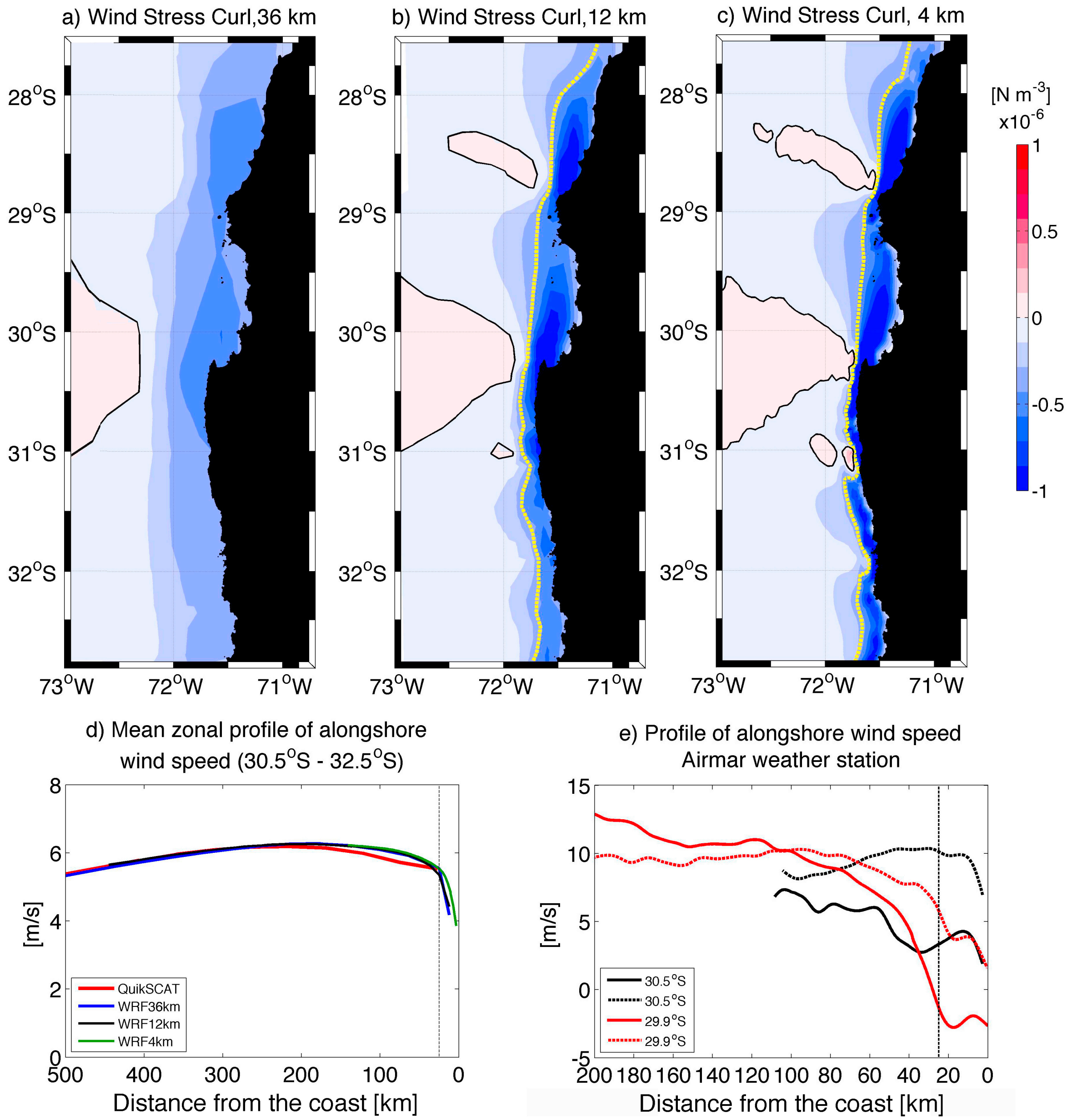
a) Wind Stress Curl,36 km
b) Wind Stress Curl,12 km
c) Wind Stress Curl, 4 km
28°S
29°S
30°S
31°S
32°S
73°W
72°W
71°W
[N m-3]
x10-6
1
0.5
0
-0.5
-1
d) Mean zonal profile of alongshore
wind speed (30.5°S - 32.5°S)
[m/s]
QuikSCAT
WRF36km
WRF12km
WRF4km
Distance from the coast [km]
e) Profile of alongshore wind speed
Airmar weather station
30.5°S
30.5°S
29.9°S
29.9°S

Figure 4.

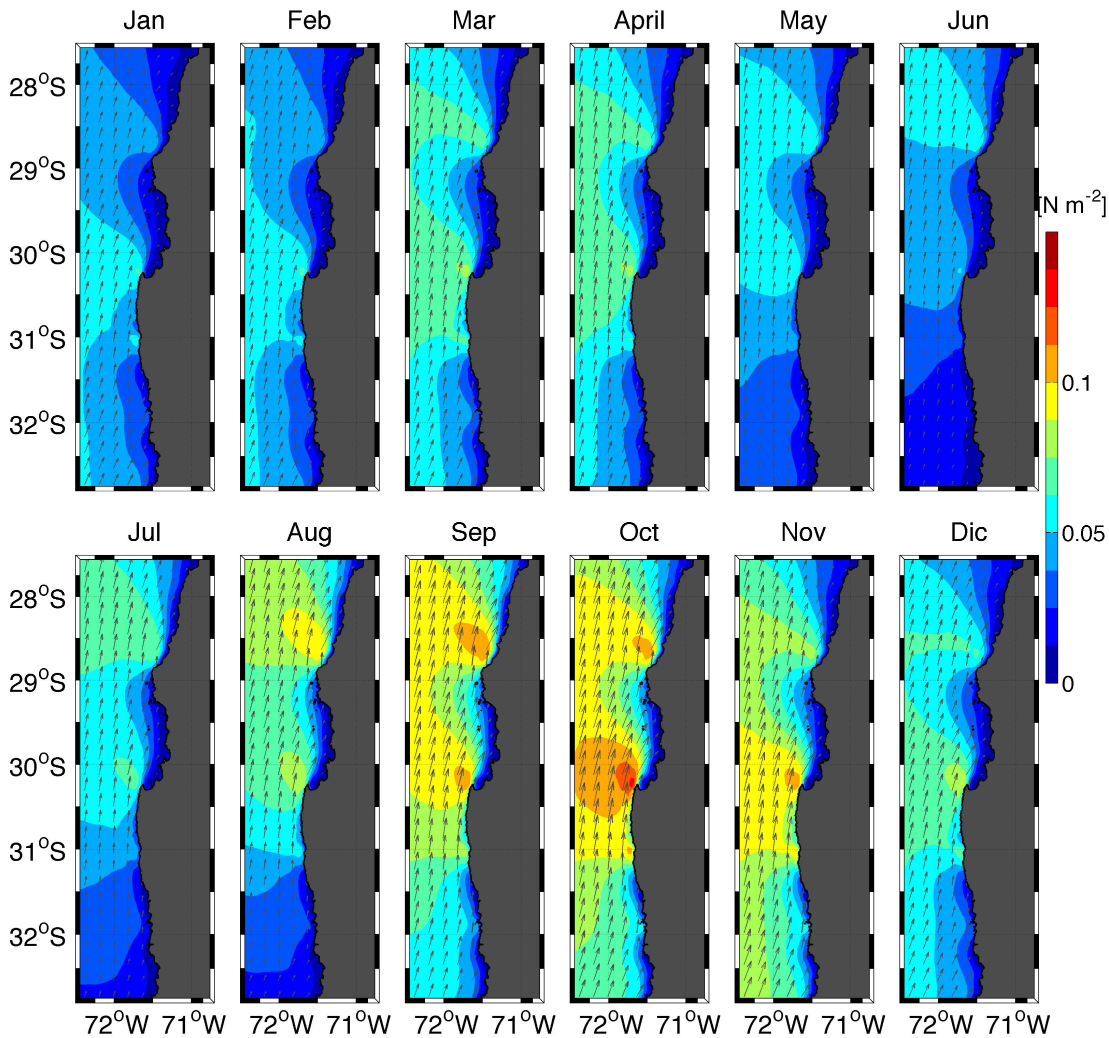

Jan
Feb
Mar
April
May
Jun
Jul
Aug
Sep
Oct
Nov
Dic
28°S
29°S
30°S
31°S
32°S
72°W
71°W
[N m⁻²]
0.1
0.05
0

Figure 5.

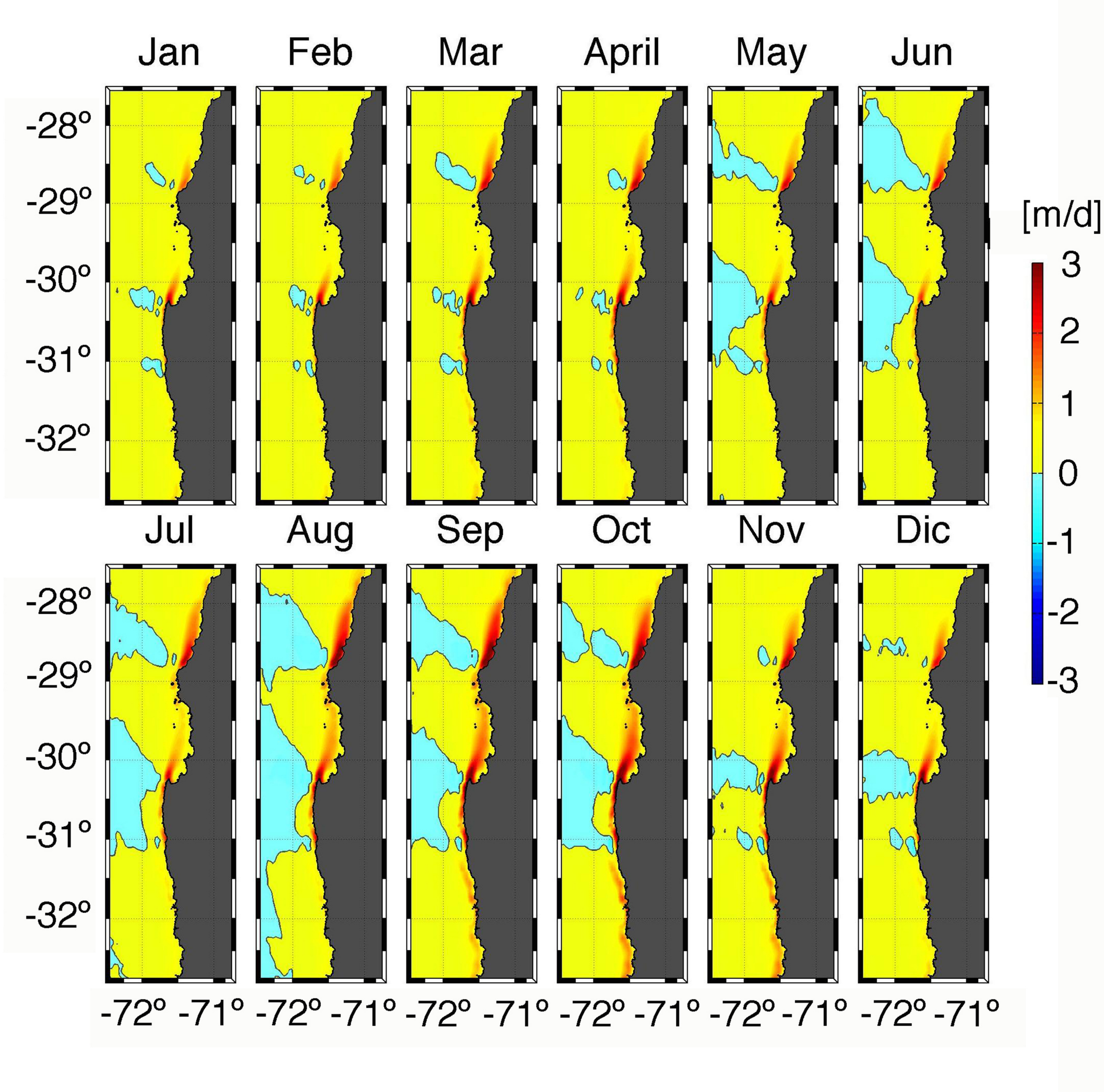
Jan
Feb
Mar
April
May
Jun
Jul
Aug
Sep
Oct
Nov
Dic
-28º
-29º
-30º
-31º
-32º
-72º -71º
[m/d]
3
2
1
0
-1
-2
-3

Figure 6.

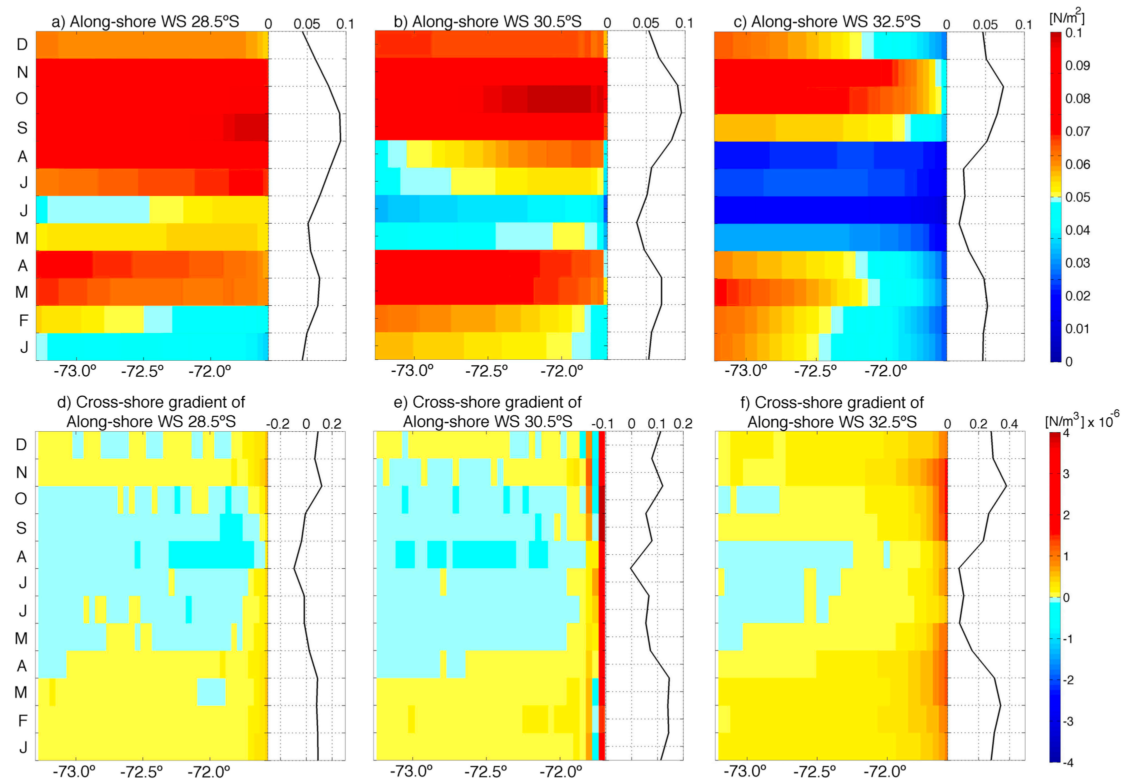
a) Along-shore WS 28.5ºS
b) Along-shore WS 30.5ºS
c) Along-shore WS 32.5ºS
[N/m²]
d) Cross-shore gradient of Along-shore WS 28.5ºS
e) Cross-shore gradient of Along-shore WS 30.5ºS
f) Cross-shore gradient of Along-shore WS 32.5ºS
[N/m³] x 10⁻⁶
D N O S A J J M A M F J
-73.0º -72.5º -72.0º

Figure 7.

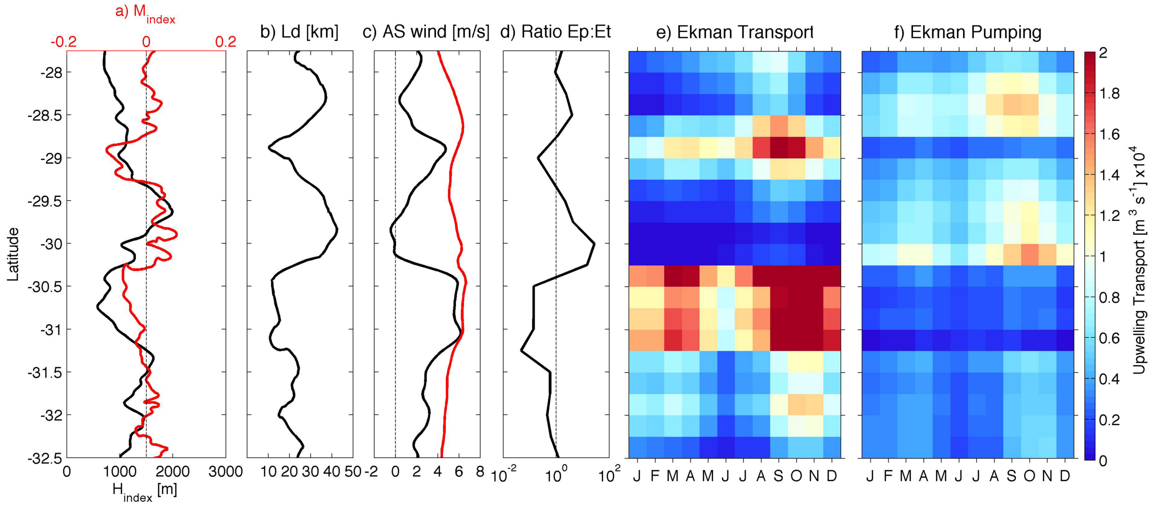

a) M_{index}
-0.2
0
0.2
b) Ld [km]
c) AS wind [m/s]
d) Ratio Ep:Et
e) Ekman Transport
f) Ekman Pumping
Latitude
-28
-28.5
-29
-29.5
-30
-30.5
-31
-31.5
-32
-32.5
0 1000 2000 3000
H_{index} [m]
10 20 30 40 50
-2 0 2 4 6 8
10^{-2} 10^{0} 10^{2}
J F M A M J J A S O N D
J F M A M J J A S O N D
Upwelling Transport [$m^3 s^{-1}$] x10^4
2
1.8
1.6
1.4
1.2
1
0.8
0.6
0.4
0.2
0

Figure 8.

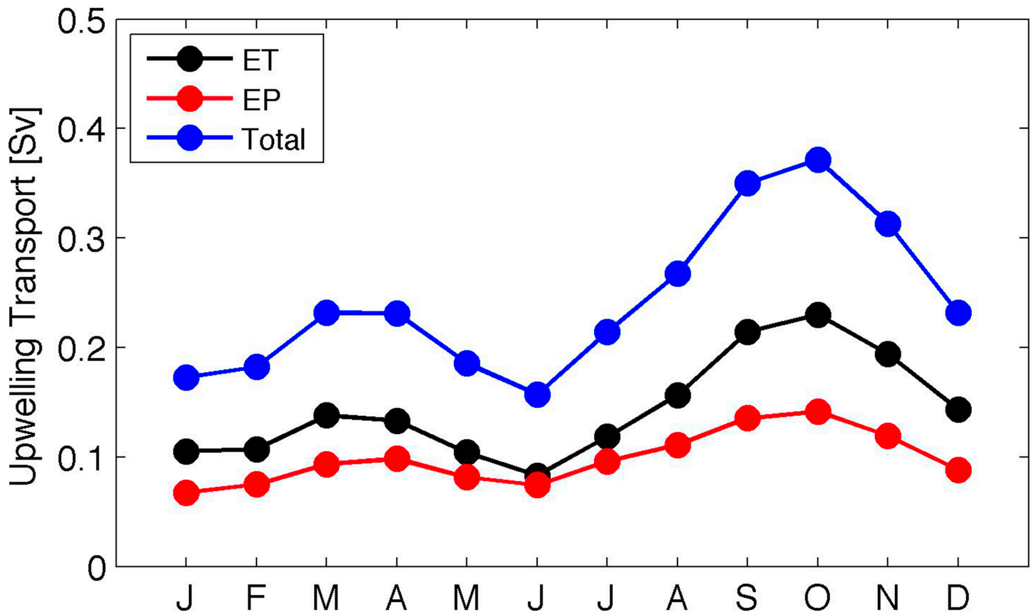

ET
EP
Total
Upwelling Transport [Sv]
0.5
0.4
0.3
0.2
0.1
0
J F M A M J J A S O N D

Figure 9.

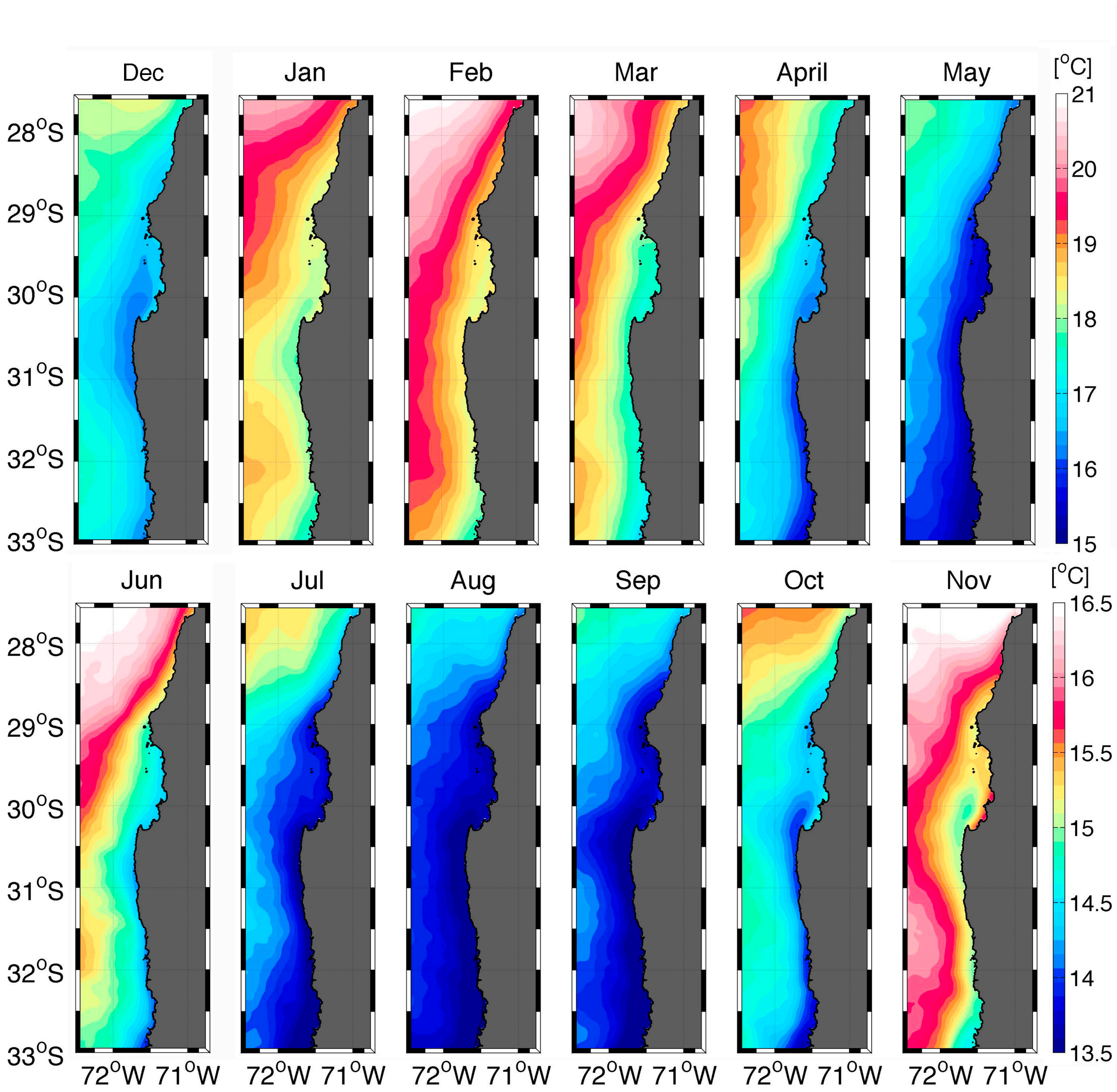
Dec
Jan
Feb
Mar
April
May
[^{o}C]
21
20
19
18
17
16
15
28^{o}S
29^{o}S
30^{o}S
31^{o}S
32^{o}S
33^{o}S
Jun
Jul
Aug
Sep
Oct
Nov
[^{o}C]
16.5
16
15.5
15
14.5
14
13.5
72^{o}W 71^{o}W

Figure 10.

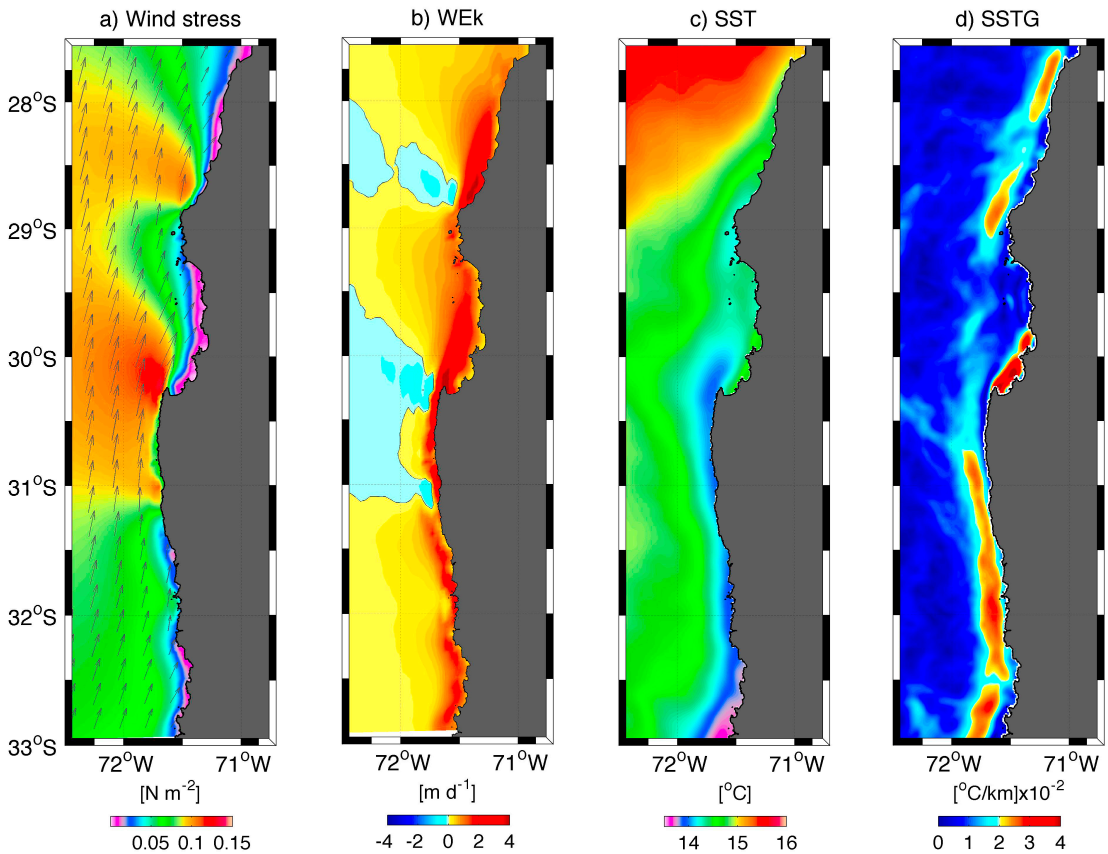

a) Wind stress
b) WEk
c) SST
d) SSTG
28°S
29°S
30°S
31°S
32°S
33°S
72°W
71°W
[N m-2]
0.05 0.1 0.15
[m d-1]
-4 -2 0 2 4
[°C]
14 15 16
[°C/km]x10-2
0 1 2 3 4

Figure 11.

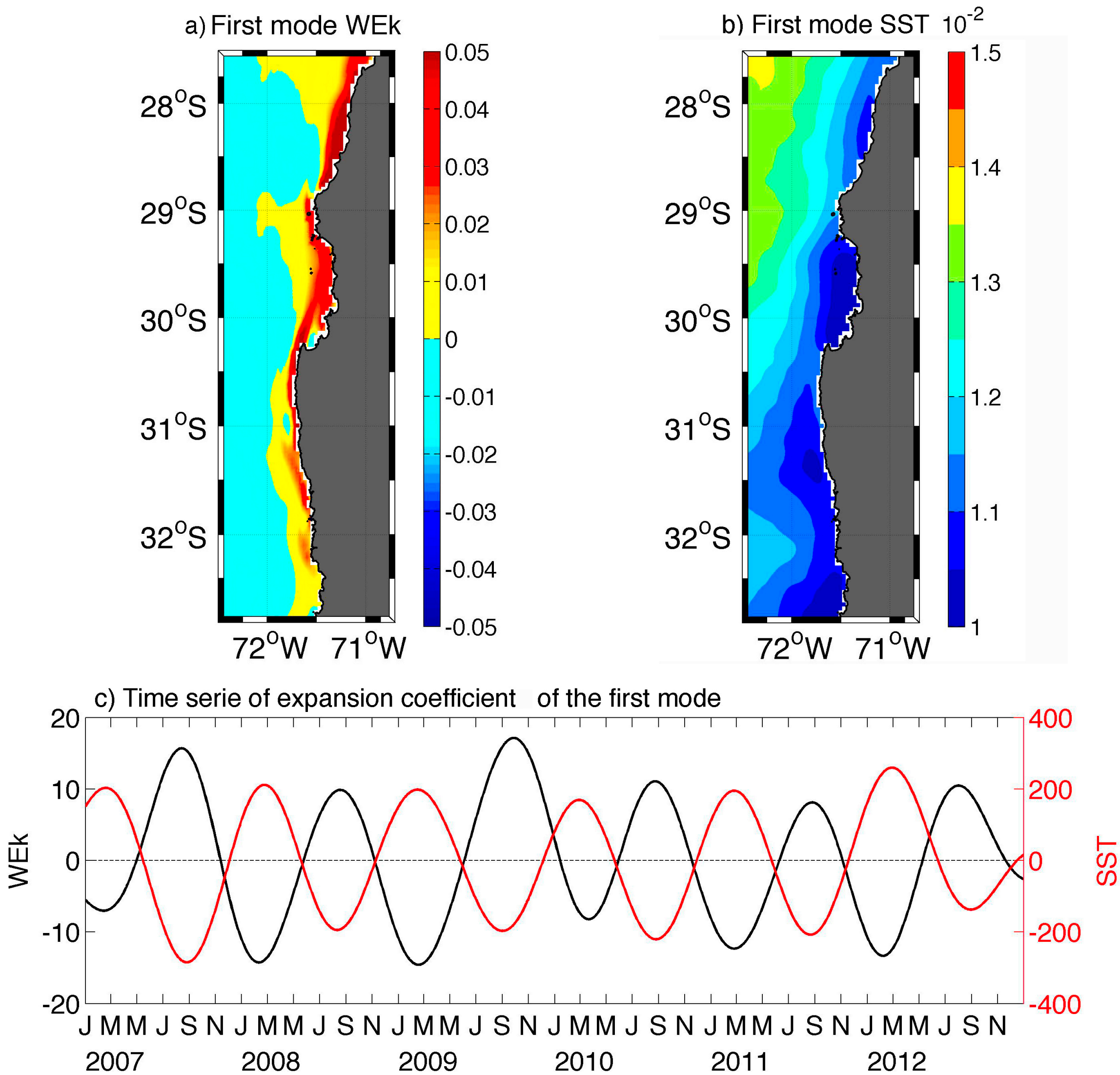
a) First mode WEk
28°S
29°S
30°S
31°S
32°S
72°W 71°W
0.05
0.04
0.03
0.02
0.01
0
-0.01
-0.02
-0.03
-0.04
-0.05
b) First mode SST 10^{-2}
1.5
1.4
1.3
1.2
1.1
1
c) Time serie of expansion coefficient of the first mode
WEk
SST
20
10
0
-10
-20
400
200
0
-200
-400
J M M J S N J M M J S N J M M J S N J M M J S N J M M J S N J M M J S N
2007 2008 2009 2010 2011 2012